Elsevier Editorial System(tm) for Materials and Design

Manuscript Draft

Manuscript Number:

Title: Compression properties of FDM structures manufactured with PLA for new mechanical designs

Article Type: Research Paper

Keywords: Additive manufacturing; FDM; Numerical simulation; Experimental tests; Plastic part design; CAD

Corresponding Author: Dr. Cristina Martin-Doñate, Ph.D.

Corresponding Author's Institution: University of Jaen

First Author: Jorge Manuel Mercado-Colmenero, Engineer

Order of Authors: Jorge Manuel Mercado-Colmenero, Engineer; Miguel Angel Rubio-Paramio, Ph.D; Mª Dolores La Rubia-Garcia, Ph.D; David Lozano-Arjona, Engineer; Cristina Martin-Doñate, Ph.D.

Abstract: This paper presents the numerical-experimental study for obtaining the mechanical properties of FDM structures manufactured with PLA subject to a stress field of uniaxial compression. A first experimental test, in accordance with the ISO 604 standard, characterizes the mechanical and elastic properties of PLA material manufactured with FDM when it is in a uniaxial compression stress field. A second experimental test analyzes the structural behavior of the study case. The characterization of the elastic behavior of the PLA material manufactured using FDM has been used for the numerical simulation of the study case by means of two empirical models. The first of the models uses the interpolation of experimental data to obtain the polynomial function of the uniaxial tension-compression curve versus nominal deformations while the second model uses Young's compression modulus according to ISO 604. The simulations results and the experimental tests show good accuracy between virtual and physical models both in the test specimens and in the study part. Additionally, the results indicate that the elastic region of the plastic material PLA manufactured with FDM can be modeled numerically as an isotropic material using the elastic properties from the experimental results of the specimens tested according to ISO 604

Graphical Abstract

Specimens manufactured with PLA and FDM

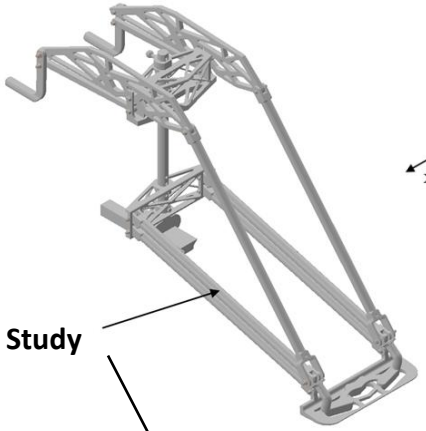

Case Study

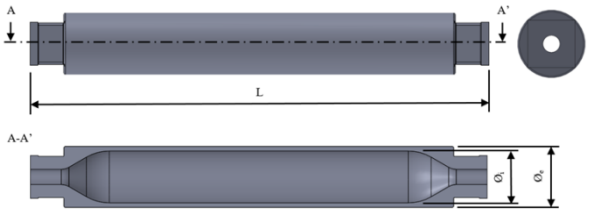

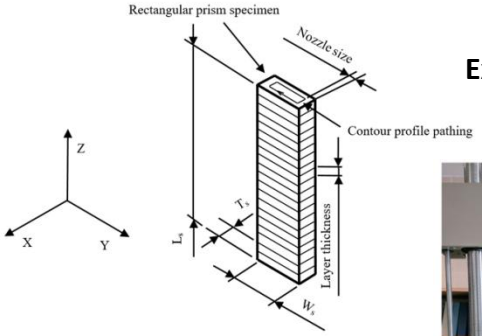

Experimental test ISO-604 standard

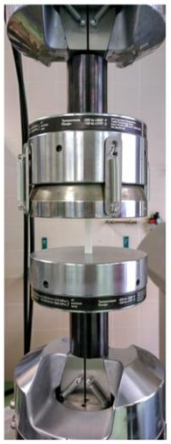

Characterization of the elastic zone for the PLA material manufactured with FDM

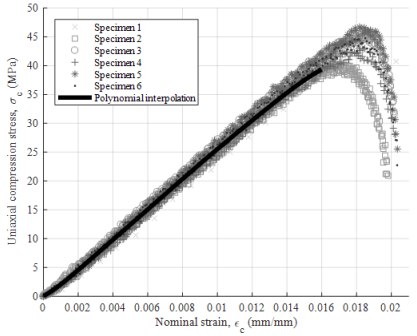

Experimental test ISO-604 standard

End Part manufactured with PLA and FDM

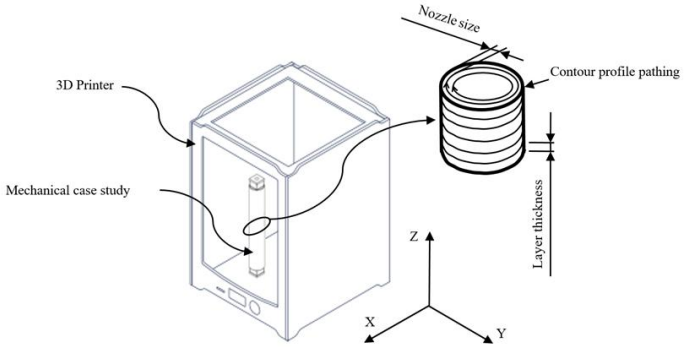

Boundary condition: Fixed support

Static input load: Uniaxial compression force

Stress field of uniaxial compression

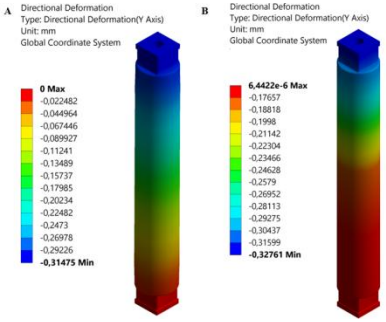

Displacements field obtained in the mechanical simulations

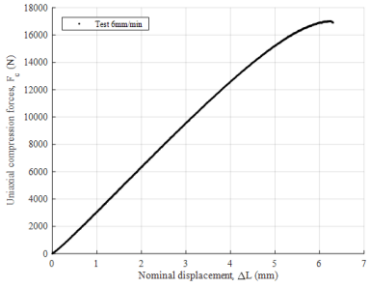

Characterization of the elastic zone Field of displacements; test

Highlights (for review)

A numerical-experimental analysis with PLA FDM structures in compression stress has been carried out

A first uniaxial compression experimental test characterizes the mechanical properties of PLA FDM specimens

A second uniaxial compression experimental test analyzes the structural behavior of the study case

The elastic mechanical properties of the PLA FDM material has been used for the study case CAE simulation

The elastic mechanical properties of the PLA FDM material can be modeled numerically as an isotropic material

Compression properties of FDM structures manufactured with PLA for new mechanical designs

Jorge Manuel Mercado-Colmenero [a], Miguel Angel Rubio- Paramio [b], Mª Dolores la Rubia-Garcia [c], David Lozano-Arjona[d], Cristina Martin-Doñate[e *]

[a , b, d, e] Department of Engineering Graphics Design and Projects. University of Jaen. Spain

[c] Department of Chemical, Environmental and Materials Engineering. University of Jaen. Spain

*Corresponding Author[e]

Campus Las Lagunillas, s/n. Building A3-210

23071 Jaen (Spain)

Phone: +34 953212821, Fax: +34 953212334

E-mail: jmercado@ujaen.es[a], marubio@ujaen.es[b], mdrubia@ujaen.es[c], dla00011@red.ujaen.es[d], cdonate@ujaen.es[e]

Abstract

This paper presents the numerical-experimental study for obtaining the mechanical properties of FDM structures manufactured with PLA subject to a stress field of uniaxial compression. A first experimental test, in accordance with the ISO 604 standard, characterizes the mechanical and elastic properties of PLA material manufactured with FDM when it is in a uniaxial compression stress field. A second experimental test analyzes the structural behavior of the study case. The characterization of the elastic behavior of the PLA material manufactured using FDM has been used for the numerical simulation of the study case by means of two empirical models. The first of the models uses the interpolation of experimental data to obtain the polynomial function of the uniaxial tension-compression curve versus nominal deformations while the second model uses Young's compression modulus according to ISO 604. The simulations results and the experimental tests show good accuracy between virtual and physical models both in the test specimens and in the study part. Additionally, the results indicate that the elastic region of the plastic material PLA manufactured with FDM can be modeled numerically as an isotropic material using the elastic properties from the experimental results of the specimens tested according to ISO 604.

Keywords: Additive manufacturing, FDM, Numerical simulation, Experimental tests, Plastic part design, CAD.

1. Introduction

Additive manufacturing (AM) is a manufacturing process that enables the production of functional parts with complex geometries and different materials, as well as individualized mass production enabling companies to produce first and effective design for not only prototypes but also successful and efficient end-products. Additive manufacturing is widely used nowadays in industrial product development [1]. The main advantage of the additive fabrication concept compared to other traditional manufacturing processes like injection molding is the ability to create almost any possible shape [2-5]. This capability is governed by the building-up layer-by layer process. The additive manufacturing technologies are playing an increasingly important role in production scenarios [6]. In particular, one of the main strong points is the production of small series components with innovative geometries not feasible using traditional technologies [7]. Additive manufacture involves the progressive addition of material to generate component geometry; this differs fundamentally from traditional, subtractive manufacture, whereby material is progressively removed from an initial geometry as required [8]. There are several available technologies based on this additive machining concept [9]: stereolithography, selective laser sintering, 3D printing, fused deposition modeling, etc. Of these, FDM, also known as fused-filament fabrication (FFF), is among the most popular. In the FDM process a feedstock filament of the raw material on a spool is fed into the extrusion head with the aid of a tractor wheel arrangement through generating extrusion pressure. The movement of the extruder by a numerical control-based code coupled with the extrusion of a semi-molten filament above the material's glass transition temperature enable the production of the desired geometry [10].

Through this technology plastics such as polycarbonate (PC), polylactic acid (PLA), acrylonitrile butadiene styrene (ABS), etc are used as raw materials. Traditionally, FDM 3D printers have been able to build parts only in thermoplastic materials such as polylactic acid (PLA) and acrylonitrile-butadiene-styrene (ABS). PLA offers better thermomechanical characteristics than ABS, having greater mechanical resistance and a lower coefficient of thermal

expansion. The latter characteristic improves the printability of PLA because it reduces the effects of warping during the printing phase. Moreover, it generates fewer health risks than ABS when printing in small and improperly ventilated spaces [11]. PLA is a bio-based plastic made up of a repeating chain of lactic acid. It is recyclable using conventional methods. In addition, PLA can be composted like other organic matter [12]. When composted, the moisture and heat in the compost pile break the PLA polymer chains apart, creating smaller polymer fragments, and finally, lactic acid. Both the smaller polymer fragments and the lactic acid act as nutrients for microorganisms in the compost. As lactic acid is widely found in nature, a large number of organisms metabolize it into carbon dioxide, water and humus, an important component of soil fertility [13-16].

In recent years, FDM has evolved from a rapid prototyping technique towards a rapid manufacturing method, changing its main purpose to producing finished components ready for use [17,18]. Indeed, this technique is particularly promising for the fabrication of a single part or in general low volume products, increasing their useful life through technical approaches such as repair or self-fabrication of parts, obtaining at the same time more sustainable socioeconomic patterns [19]. This trend highlights the need for a deeper understanding of the mechanical properties and the behavior of parts produced with FDM. FDM is a complex process with a large number of parameters that influence product quality and material properties, and the combination of these parameters is often difficult to understand [20,21]. Printing parameters such as build orientation, layer thickness, raster angle, raster width, air gap, infill density and pattern and feed rate have a substantial effect on the quality and performance of FDM printed parts [18,20,22-24]. Since mechanical properties are crucial for functional parts, it is absolutely essential to examine the influence of process parameters on mechanical performance [25-27].For this reason many researchers have focused their efforts on this area to determine the effect of process parameters, where mechanical properties as important indices are measured and compared in order to evaluate the quality of printed parts [28-30]. Several papers deal with the anisotropic characteristics of FDM parts, analyzing the properties of the material in a state of tension, flexion and compression. More specifically Rodriguez et al. [31] introduce a strategy for optimizing the design of Fused-Deposition Manufacture of ABS P400 components, analyzing stiffness and strength under a given set of loading conditions. In this research a mathematical model of the structural system is linked to an approximate minimization algorithm to find the settings of manufacturing parameters which optimize the mechanical performance of the component. Ahn et al. [32] characterize the properties of ABS parts fabricated by FDM using a Design of Experiment (DOE) approach, analyzing the process parameters like raster orientation, air gap, bead width, color, and model temperature, obtaining tensile strengths and compressive strengths and comparing these with the analysis of injection molded specimens. Some researchers have used the Taguchi method to study the optimal process parameters for a fused deposition modeling (FDM) rapid prototyping machine. Anitha et al.[26] asses the influence of the process parameters on the quality characteristics of the prototypes manufactured with FDM technology. Lee et al. [33] analyzed a set of FDM parameters like layer thickness, raster angle and air gap, studying their influence on the elastic performance of an ABS prototype. Croccolo et al. [34] studied the effects of the Fused Deposition Modelling production parameters on the tensile strength and on the stiffness of the components made of ABS-M30, tackling the question from both the experimental and the analytical points of view. Domingo- Espín et al. [22] proposed a model to simulate FDM parts, correlating a finite element analysis (FEA) simulation with physical testing.

Casavola et al. [20] described the mechanical behavior of FDM parts through the classical laminate theory (CLT) and in a later study [35] analyzed the residual stress of FDM parts made of ABS by employing the hole-drilling measure method. Tymrak et al. [18] quantify the basic tensile strength and elastic modulus of printed components using realistic environmental conditions for standard users of a selection of open-source 3-D printers. Tanikella et al. [36] investigated the mechanical properties of 3D printed parts using a commercial open-source3D printer for a wide range of materials, testing the samples for tensile strength. Kuznetsov et al. [37] studied the influence of geometrical parameters of fused deposition modeling (FDM) on printed part strength for open source desktop 3D printers and PLA material. Wittbrodt et al. [38] determined the effect of color and processing temperature on PLA material properties in various colors. More recently Chacón et al. [39] characterized the effect of build orientation, layer thickness and feed rate on the mechanical performance of PLA samples manufactured with a low cost 3D printer. Puigoriol-Forcada et al [10] presented an experimental investigation of the influence of part build orientation on the flexural fatigue behaviors of fused-deposition modelling (FDM) processed polycarbonate (PC) parts. Torres et al. [40] presented the influences of key processing parameters on the resulting material properties of fused-deposition-modeled (FDM) polylactic acid (PLA) components tested in torsion.

Plastic polymers are characterized by their good performance in comparison with high compressive strengths, this mechanical feature being a great advantage when designing mechanical assemblies manufactured with FDM technology. Uddin et al. [41] presented a comprehensive experimental study exploring the influence of key printing parameters on mechanical properties and failure mechanisms of acrylonitrile butadiene styrene (ABS) material. Upadhyay et al. [42] focused on the effect of build direction on the mechanical properties of acrylonitrile butadiene

styrene ABS P400 part specimens analyzing tensile and compressive strength, Izod impact and hardness. Sood et al. [43] focused on extensive study to understand the effect of five important parameters such as layer thickness, part build orientation, raster angle, raster width and air gap on the compressive stress of test specimens. Lee et al. [44] investigated the measurement of the anisotropic compressive strength of rapid prototyping parts. However, the research carried out so far has not been focused on the analysis of the influence of manufacturing parameters on PLA manufactured parts subject to compression uniaxial loads. Another important aspect to emphasize is that FDM designers and users should take into account the differences between the mechanical properties of bulk polymers presented by producers in the material specifications sheet and the mechanical properties of testing specimens and manufactured end-parts. At the same time, this literature review identified only the study of Lee et al. [33] which focused on the evaluation of FDM process parameters and their optimization for improving the mechanical performance of a real part. In the literature the dependence between FDM process parameters values and mechanical behavior has been studied mainly for test specimens alone. Therefore, further research should evaluate the mechanical performance on FDM end-parts and thus their suitability for particular applications [45].

The design of parts for agricultural machinery is usually adapted to the needs of the farmer so that a custom design is considered adequate in most cases. At an industrial level, some companies are starting to manufacture plastic parts for agricultural machinery using FDM technology [46]. Among the many advantages of using this technology are a reduction in manufacturing costs, shorter delivery times, independence from the supplier, the possibility of using sustainable materials, etc. [47]. Additionally, this technology allows the farmer to be independent from third parties in the field of repairing machinery parts, enabling full-time harvesting at the most critical moments of the campaign. The plastic parts manufactured by FDM offer the possibility of changing many agricultural operations, making possible more innovative 3D designs impossible to manufacture with traditional methods. In this way any producer can make a prototype of a plastic part, test it and manufacture it directly without the need for expensive steel injection molds. Another additional benefit of the use of plastic parts manufactured with FDM is the possibility of developing agricultural areas with few resources [12]. The lack of manufacturing resources is one of the main problems of developing countries, added to the high costs of acquisition and shipment of the pieces and the cost of the material. In this way, printers enable sustainable agriculture that helps the development of disadvantaged countries [48].

Based on the problems outlined above this paper presents a numerical-experimental study for obtaining the mechanical properties of FDM structures manufactured with PLA, subject to uniaxial compression stress states. The element under study consists of a bar with circular hollow section belonging to a mechanical device for the displacement of the collection sheets in the process of olive harvesting. Experimental tests have been carried out with the specimens test as well as with the end part, all of them following the ISO 604 standard. FEA simulations have been carried out with different elastic models, obtaining as a result the validation of the physical model proposed. The data on the uniaxial compression force as well as the nominal displacements for the experimental test and the numerical simulations of the study case show that the structural behavior is not compromised for the scenario of loads and boundary conditions required by the design. The device in which the end study part has been included is recyclable and can be manufactured by the farmer himself, being able to repair the device autonomously without relying on suppliers. The FDM additive manufacturing process allows farmers to design customized devices for their needs, incorporating environmentally friendly materials such as PLA while maintaining the functional performance of the device.

2. Geometrical and functional description of the FDM mechanical case study

In this section, the geometry of the FDM mechanical case study is presented and described. Additionally, factors that intervene in the selection of material for 3D printing using FDM techniques, the boundary conditions and load scenario to which this mechanical element is subject are presented. As shown in Fig.1, this mechanical element is part of a mechanism for the optimization of agricultural processes [49].

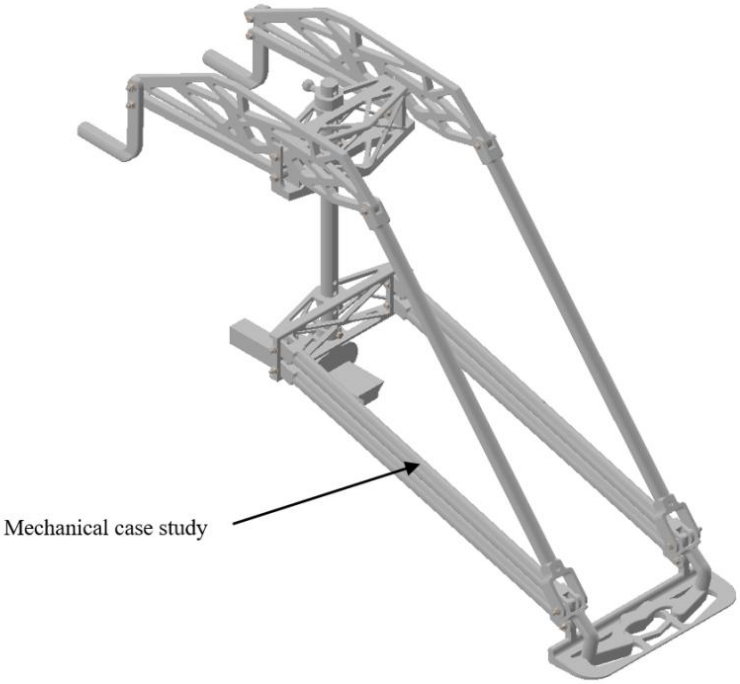

Fig. 1.- Geometry of the mechanical assembly manufactured with FDM for the optimization of agricultural processes.

This mechanical element is a bar with a constant circular ring section throughout its domain. The bar has at its ends some anchors that allow the correct assembly of the bars with the rest of the mechanical assembly. The material used for the manufacture of the mechanical assembly with FDM 3D printing is a polylactic acid type plastic (PLA). This plastic being biodegradable allows the mechanical assembly to be sustainable. That is, it can be eliminated as organic waste and in the presence of microorganisms can serve as organic fertilizer, which can be interesting also for agricultural applications. Table 1 shows the physical, mechanical and manufacturing properties of the PLA commercial material yarn, manufactured by Smart Material 3D [50], used for printing the mechanical element presented.

PLA Properties	Value	Units
Density	1,24	g/cm^3
Tensile strength MD	110	MPa
Tensile strength TD	114	MPa
Tensile modulus MD	3309	MPa
Tensile modulus TD	3861	MPa
Elongation at break MD	160	%
Elongation at break TD	100	%
Heat deflection temperature	65	ºC
Vicat softering temperature	85	ºC
Print temperature	220±10	ºC
Hot pad	0-60ºC	ºC

Table 1.- Physical, mechanical and printing properties for PLA material manufactured with FDM technology.

The mechanical element under study is subjected to a tensional state of pure uniaxial compression. That is to say, the load scenario to which the mechanical element under study is subjected means that the mechanical stresses it undergoes are pure uniaxial compression. In this way, the object of this study is the analysis of the structural behavior of the main geometry of the mechanical element for a tensional state of pure uniaxial compression. Fig.2 shows in detail the geometry of the mechanical element under study. As can be seen, the ends of the element have been modified to adapt the geometry to the measuring instruments and the uniaxial compression testing machine, while the geometry and tubular section of the study area of the mechanical element remain constant.

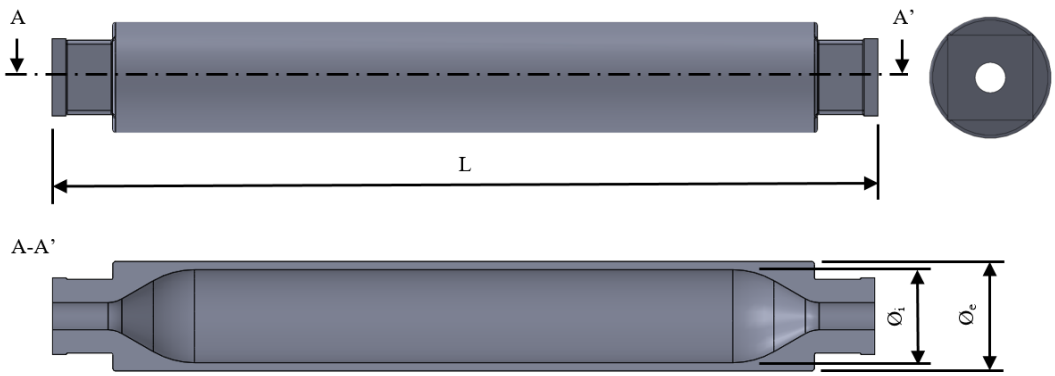

Fig. 2.- Geometry of the mechanical case study.

The dimensions of the mechanical element under study (see Fig.2) are presented in Table 2. The geometrical variables $Ø_i$ (inner diameter) and $Ø_e$ (outer diameter) which determine the cross section of the mechanical element have been dimensioned according to the mechanical properties of the PLA material (see Table 1). In this way, starting from the uniaxial compression force to which the mechanical element under study and the tensile yield stress of the plastic material are subjected, the magnitude of the cross-sectional area of the mechanical element is determined by a classical structural analysis (see Eq. 1)

$$\sigma_y \geq \frac{F_c \cdot \gamma_s}{A_{cross}} \tag{1}$$

Where σ_y [MPa] represents the tensile yield stress of the plastic material, F_c [N] represents the uniaxial compression force to which the mechanical element is subjected, A_{cross} [mm^2] represents the area of the cross section of the mechanical element and γs represents a structural safety coefficient equal to 1.5.

Variable	Description	Units	Value
$Ø_e$	Outer diameter of the mechanical element	mm	40
$Ø_i$	Inner diameter of the mechanical element	mm	34
L	Length of the mechanical element	mm	300

Table 2.- Geometrical variables that define the mechanical element under study.

Fig.3 shows the load scenario and the boundary conditions to which the mechanical element under study is subjected. As can be seen, it is a pure uniaxial compressional tension state where the maximum uniaxial compressive force that the mechanical element bears during the nominal operation of the mechanism, to which it belongs, is equal to 900 N. The application of this uniaxial compression force is performed at the opposite end of the mechanical element where the boundary conditions are defined. The boundary condition established for the structural analysis of this mechanical element is either fixed or of the embedment type.

Fig. 3.- Boundary conditions and definition of the loads borne by the mechanical element.

Finally, the manufacture, using FDM 3D printing techniques, of the mechanical element under study has been carried out with a commercial 3D printer Ultimaker 2+ Extended [51]. The printing dimensions of this commercial 3D printer are: 223 mm on the X axis, 223 mm on the Y axis and 305 mm on the Z axis. Therefore, given the dimensions of the mechanical element the manufacturing is carried out along the longitudinal axis, ie the Z axis (MD direction) (see Fig. 4). Authors such as [42] conclude that the structural behavior and the compressive strength of the elements

manufactured along the longitudinal direction (Z axis) improves with respect to those manufactured along the transversal direction (X or Y axis).

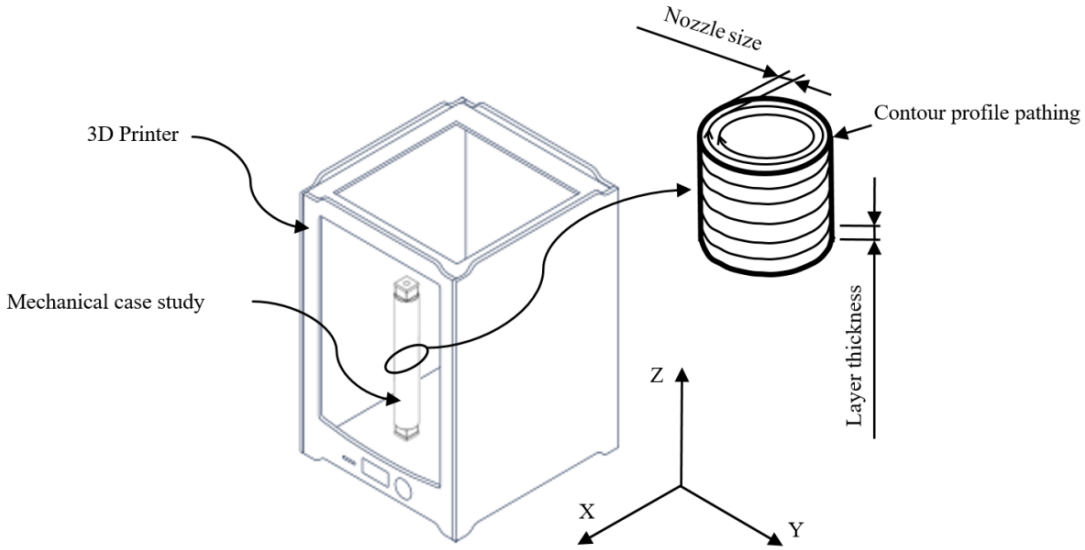

Fig. 4.- Configuration of the 3D printing process of the mechanical element under study.

As shown in Fig.4, the 3D printing strategy used to generate the different layers during the manufacturing process has been that of contour profile. Authors such as [41] conclude that for a manufacturing by deposition of layers along the Z direction, the orientation or printing strategy used for each layer has a negligible effect on compressive properties given the symmetry that occurs in the cross section of the mechanical element. Table 3 shows the magnitude of the parameters defined for the configuration of the manufacturing process. For the correct manufacture of the mechanical element under study and the optimization of the printing process the geometric design of this element is adapted to the criteria and requirements of additive manufacturing using the FDM technique This allows the geometry to be printed completely without needing auxiliary supports, minimizing in this way the quantity of material used during the manufacturing process.

Manufacturing parameters	Value	Units
Layer height	0,2	mm
Nozzle size	0,4	mm
Infill density	100	%
Print speed	50	mm/s
Travel speed	120	mm/s

Table 3.- Parameters of manufacture used for the manufacture of the elements of the present study.

3. Experimental set-up and methodology

In this paper two types of experimental uniaxial compression tests are described for mechanical elements manufactured using additive manufacturing techniques of the FDM type. The first type of test focuses on the characterization of the mechanical and elastic properties of the 3D PLA plastic printing material, according to the conditions and requirements established in the ISO-604 standard (2003) [52]. On the other hand, in the second test the structural behavior of the mechanical element object of study is analyzed before a tensional state of uniaxial compression, evaluating the compressive stiffness of the mechanical element, its compression yield stress, the field of movements and strengths along its elastic behavior until reaching the compression yield stress and the ultimate yield stress. Subsequently, with the information of the mechanical and elastic properties of the PLA material, a set of numerical simulations with different elastic models has been carried out for the mechanical element under study. In this way, the results of the numerical simulations are validated by the results obtained in the second experimental test on the mechanical element under study.

According to the standard ISO-604, to carry out the characterization of the mechanical and elastic properties to uniaxial compression of the plastic material for 3D printing PLA, specimens with rectangular prism geometry should

be tested experimentally (see Fig.5). Table 4 shows the dimensions of the specimens, both for the calculation of the compression elastic modulus and for the calculation of yield stress compression. The magnitude of the manufacturing parameters used for the manufacture of the specimens is shown in Table 3, and these are analogous to those used for the manufacture of the mechanical element under study in this paper.

Measurement parameter	Length, L_s	Weidth, W_s	Thickness, T_s	Unit
Compression Young modulus	50±2	10,0±0,2	4±0,2	Mm
Compression yield stress	50±2	10,0±0,2	4±0,2	Mm

Table 4.- Dimensions of the specimens used for the characterization of PLA compression material.

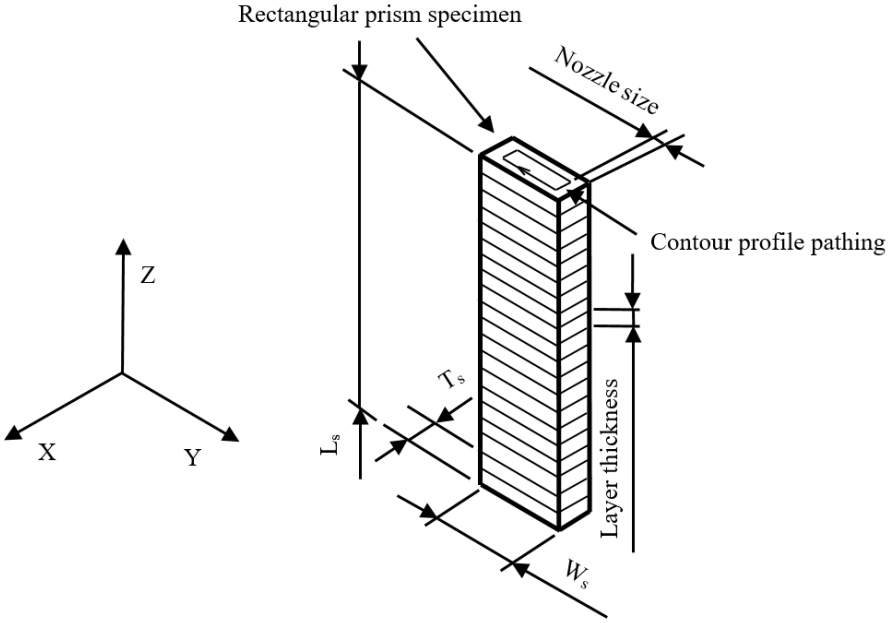

Fig. 5.- Configuration of the 3D printing process for the specimens analyzed in the experimental test.

The standard applied for this type of test, ISO-604, recommends testing at least 5 specimens for each main direction in which we wish to obtain the elastic and mechanical properties of the plastic material. Therefore, in order to validate the experimental tests according to this standard a total of 6 specimens with the same geometrical and manufacturing characteristics have been tested.

Fig.6 shows a specimen prepared for testing on the compression machine. As can be seen, the specimen is placed between the surfaces of the compression plates, ensuring that the specimen end surfaces are parallel to the compression plates surfaces. Then, before starting the test the test machine is adjusted so that the surfaces are not in contact. The compression speed used for the test of the different specimens has been 1 mm/min, according to the criteria established in standard ISO-604 (see Eq.2), and this speed has been constant from the start of the uniaxial compression test to the break instant of each specimens.

$$v = 0{,}02 \cdot L_s \tag{2}$$

Where v [mm / s] represents the compression speed of the test and L_s [mm] the length of the specimens tested.

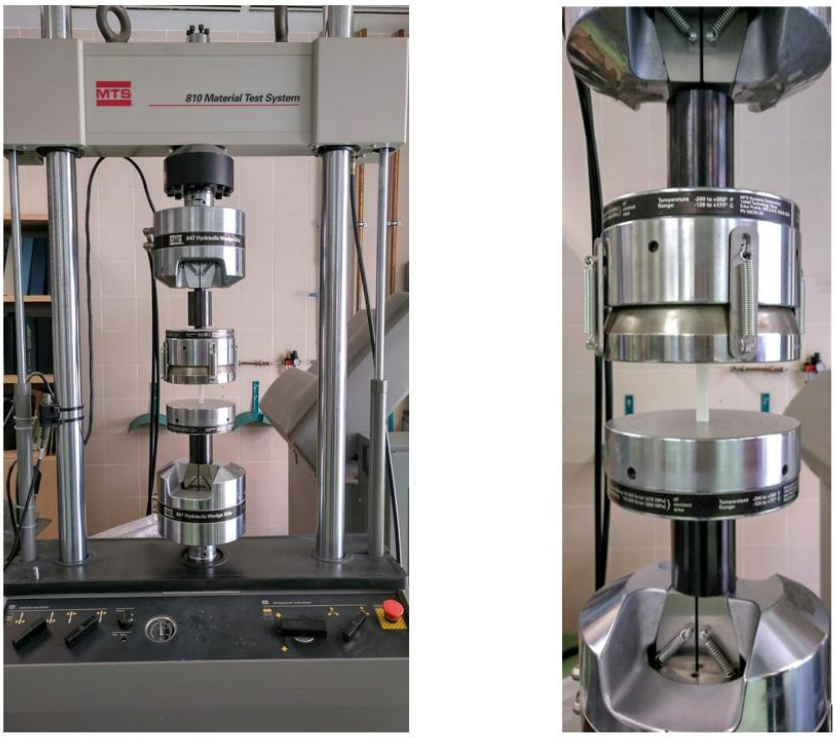

Fig. 6.- Uniaxial compression test of the specimens. A) Test machine, MTS-810. B) Compression plates and specimen.

The compression machine used for the execution of the experimental tests is MTS-810 (see Fig.6), which meets the ISO-5893 standard. This machine has two hardened steel compression plates with a flatness between both plates of 0.02 mm, and parallel to each other in a perpendicular plane to the axis of the compression load. The compression machine has a mechanism capable of displaying and recording the uniaxial compression load that each specimen supports during the tests. It also incorporates a mechanism capable of displaying and recording the distance between the surfaces of the compression plates, allowing us to define both the tensional state and the nominal deformation without inertial slowing of the test speed of 1 mm / min. of the specimens during the tests

Fig.7 shows the graph of uniaxial compression force versus the field of nominal compression displacements to which the specimens are subjected during the compression test. As shown, these parameters were recorded until the moment of breakage or structural failure of each specimen. From these parameters of compression forces and nominal displacements, the uniaxial compression stress and the nominal strain (see Fig.8) are determined according to Eq.3 and Eq.4 , in accordance with standard ISO-604.

$$\sigma_c = \frac{F_c}{A_{\text{cross specimen}}} \tag{3}$$

$$\varepsilon_c = \frac{\Delta L}{L_s} \tag{4}$$

Where σ_c [MPa] represents the uniaxial compression stress, F_c [N] the uniaxial compression force, $A_{\text{cross specimen}}$ [mm^2] represents the cross sectional area (assumed to be constant throughout the compression test), ε_c [mm / mm] represents the nominal deformation of compression, ΔL [mm] represents the nominal displacement of the specimen and L_s [mm] represents the initial length of the specimen.

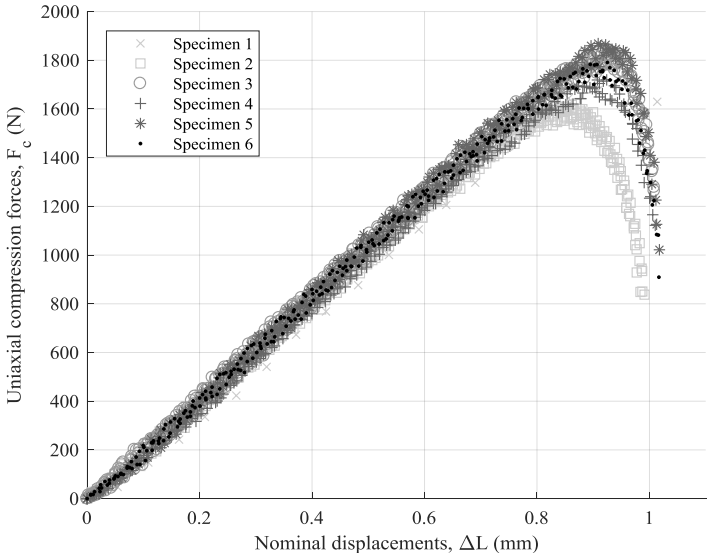

Fig. 7.- Uniaxial compression force versus nominal displacements for the specimens tested.

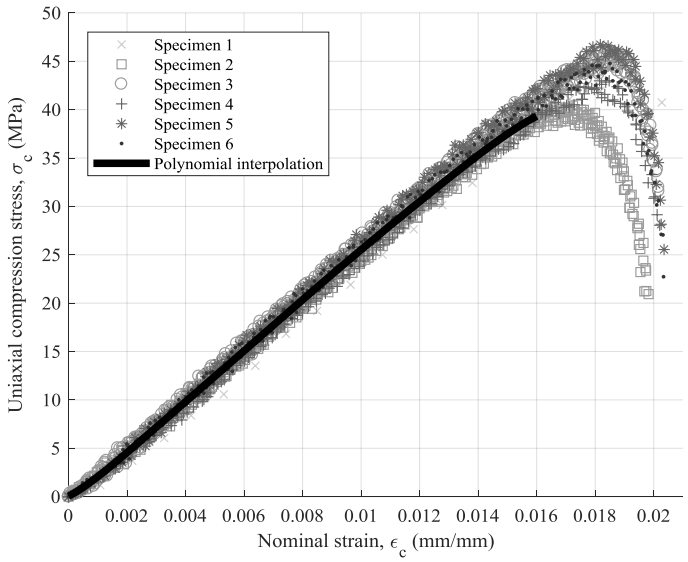

Fig. 8.- Uniaxial compression stress versus nominal strains for the specimens tested.

As shown in Fig.8, the stress-strain curve (σ_c-ε_c) presents a linear-elastic behavior until reaching the compression yield stress. From this value, the fracture process of the specimens begins and the curve descends until reaching the fracture yield stress. As shown in Fig.9, the fracture that occurs in the specimens is of a brittle type. In most of the specimens analyzed the fracture is not caused by the collapse of the plastic material, but by the separation between the central plastic filament layers of the specimen. That is to say, when exceeding the compression yield stress the central layers of plastic filament begin to separate until reaching the yield stress fracture, from which a complete separation between layers of material is produced and therefore the fracture of the specimen.

From the data of uniaxial compression stress and nominal deformations obtained for the 6 specimens tested, a polynomial interpolation is performed for the elastic regime of the curve presented in Fig.8.The interpolation is achieved by means of a polynomial of degree 8 (see Eq.5). Table 5 shows the results obtained in the interpolation of the uniaxial compression stress curve versus nominal deformations.

$$\sigma_c(\varepsilon_c) = P_1 \cdot {\varepsilon_c}^8 + P_2 \cdot {\varepsilon_c}^7 + P_3 \cdot {\varepsilon_c}^6 + P_4 \cdot {\varepsilon_c}^5 + P_5 \cdot {\varepsilon_c}^4 + P_6 \cdot {\varepsilon_c}^3 + P_7 \cdot {\varepsilon_c}^2 + P_8 \cdot \varepsilon_c + P_9 \quad (5)$$

Interpolation parameters	Value
Coefficients (95% confidence bounds):	
P1	$-3{,}465\cdot10^{17}$
P2	$2{,}394\cdot10^{16}$
P3	$-6{,}613\cdot10^{14}$
P4	$9{,}253\cdot10^{12}$
P5	$-6{,}803\cdot10^{10}$
P6	$2{,}386\cdot10^{8}$
P7	$-2{,}266\cdot10^{5}$
P8	2131
P9	-0,004
Goodness of fit:	
SSE	113,1
R-Square	0,999
Adjusted R-Square	0,999
RMSE	0,2741

Table 5.- Results of the polynomial interpolation of the uniaxial curve compression stress against nominal deformations

Thus, the elastic and mechanical properties of the PLA plastic material are determined by 3D printing manufacturing for each of the specimens tested. According to the ISO-604 standard, the compression Young modulus is determined based on two pairs of uniaxial compression stress values corresponding to nominal deformations equal to 0,0025 and 0,0005 (see Eq.6).

$$E_c = \frac{\sigma_c(\varepsilon_c = 0{,}0025) - \sigma_c(\varepsilon_c = 0{,}0005)}{0{,}0025 - 0{,}0005} \tag{6}$$

From the compression Young modulus of each tested specimen (see Table 6), the compression Young modulus of PLA plastic material for 3D printing has been calculated as the arithmetical mean of the values obtained for the specimen. Table 6 shows the elastic and mechanical properties of PLA plastic material manufactured with 3D printing.

Compression properties	Units	S1	S2	S3	S4	S5	S6	Arithmetic average	Typical deviation
Young modulus, E_c	MPa	2304,7	2363,3	2903,1	2319,0	2899,3	2381,3	2528,5	290,087
Yield stress, σ_y	MPa	44,09	40,59	46,08	42,99	46,72	44,77	44,2	2,223
Fracture stress, σ_f	MPa	40,76	20,94	31,58	28,05	25,54	22,73	28,3	7,196

Table 6.- Elastic and mechanical properties of PLA plastic material for each specimen.

In this way, the characterization of the elastic regime of PLA plastic material for 3D printing is carried out by means of two empirical models. The first by interpolation through a polynomial function of the uniaxial compression stress curve versus nominal deformations, and secondly by obtaining the Young modulus in compression according to the guidelines established in the ISO-604 standard. Both empirical models are compared and used for the definition of the numerical simulations of the mechanical element which is the object of study of the present paper.

As shown in Table 6, there is a notable dispersion in the results of the compression fracture stress parameter σ_f. This is because the specimen fracturing process is an unstable state that requires increasing the frequency of force and displacement data recording by the test machine to analyze in detail the exact moment of breakage or collapse of the specimen. Since the main objective of the present article is to evaluate the elastic behavior of the PLA plastic material, ie the compression elastic modulus, the recording frequency of force and displacement data of the MTS-810 test machine remains constant.

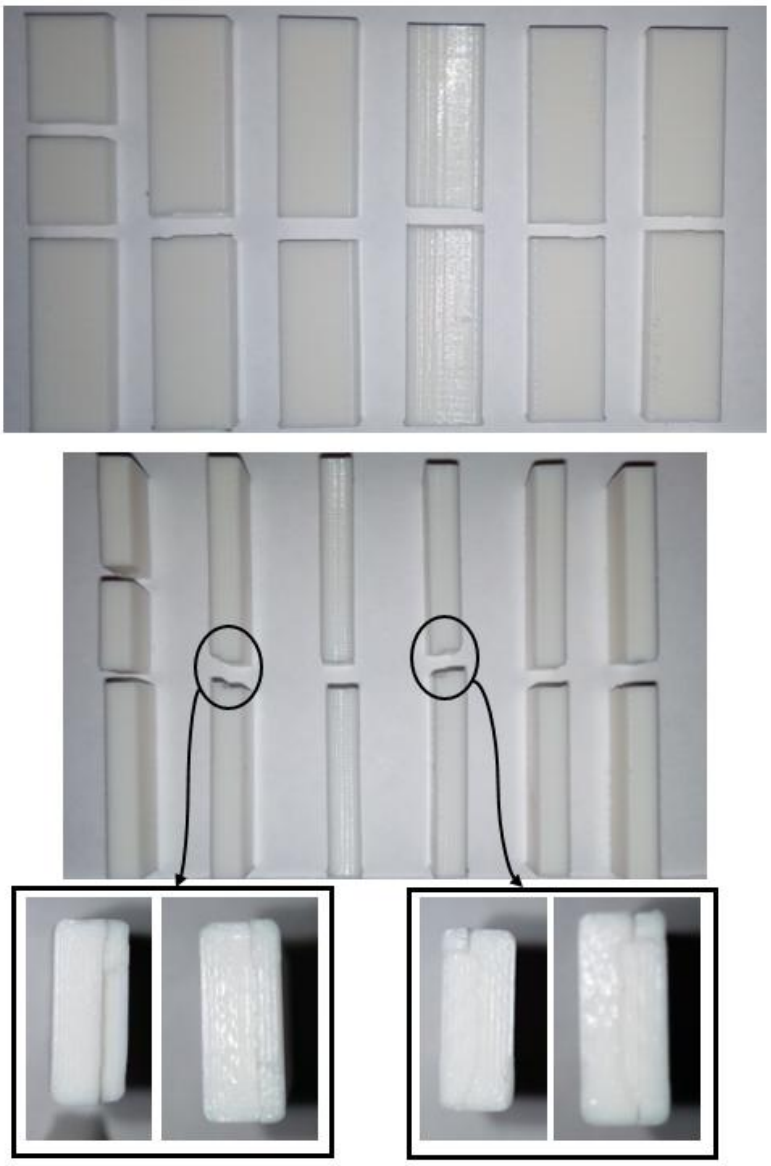

Fig. 9.- Failed tensile test specimens.

Finally, after conducting the experimental tests of the different specimens we proceeded to analyze experimentally the structural behavior of the mechanical element. Analogous to the tests carried out for the specimens, the uniaxial compression analysis of the mechanical element (see Fig.2) was performed on the MST-810 test machine (see Fig.10). The compression speed used was 6 mm / min, according to Eq.2, this speed being constant from the beginning of the uniaxial compression test until the moment of rupture of the mechanical element. Fig.11 shows the graph of uniaxial compression force versus the field of nominal displacements of compression to which the mechanical element was subjected during the compression test. As shown, these parameters were recorded until the moment of breakage or structural failure. From these parameters of compression forces and nominal displacements the uniaxial compression stress and the nominal strain (see Fig. 12) are determined according to Eq.3 and Eq.4. Table 7 shows the magnitude of the uniaxial compression force and the maximum nominal displacement reached at the breaking point of the mechanical element. As can be observed, the fracture of the mechanical element is brittle because the compressive yield stress is close to the fracture yield stress.

Fig. 10.- Uniaxial compression test of the mechanical element under study.

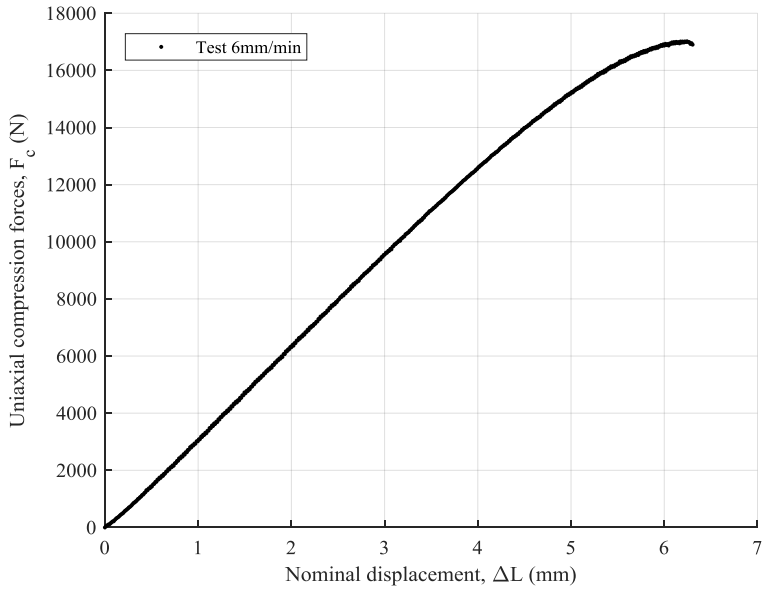

Fig. 11.- Uniaxial compression force versus nominal displacements for the mechanical element tested.

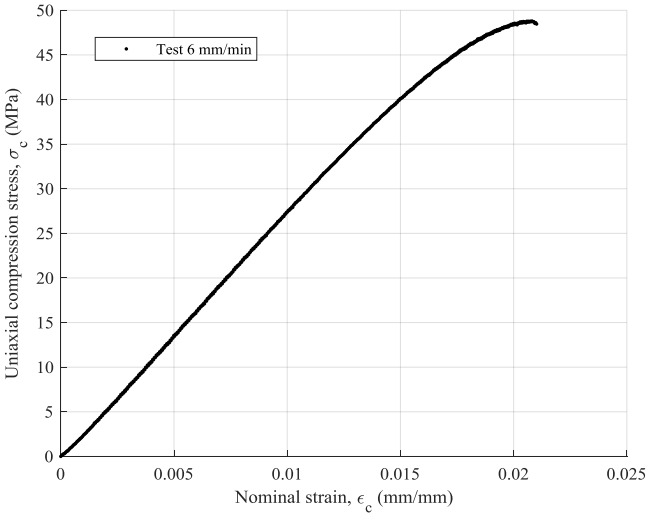

Fig. 12.- Uniaxial compression stress versus nominal deformations for the mechanical element tested.

Compression properties	Units	Value
Maximum uniaxial force	N	16091,0
Maximum nominal displacement	mm	6,304
Yield stress, σ_y	MPa	48,78
Fracture stress, σ_f	MPa	48,47

Table 7.- Mechanical properties of the study object obtained in the uniaxial compression test.

4. Numerical method

Ansys Mechanical [53] was the commercial software used to simulate numerically the structural behavior of the mechanical element under study under the scenario of loads and boundary conditions that are presented in Fig.3 and Fig.13.In the numerical simulations it is assumed that the established models are linear and static. To define the material of the numerical simulations, the empirical models have been established from the experimental results of the specimen tests. On the one hand, in the first set of numerical simulations PLA plastic material is defined as an elastic isotropic material, where the value of the compression Young modulus employed is constant and equal to 2528.5 MPa (see Table 6). The coefficient of Poisson is equal to 0.38 (Parameter established by the manufacturer of the plastic material).On the other hand, in the second set of numerical simulations the elastic properties of the material are defined by importing the numerical values of the polynomial function used to interpolate the elastic area of uniaxial compression stress versus the nominal deformations obtained from the specimens´ experimental tests (see Fig.8).

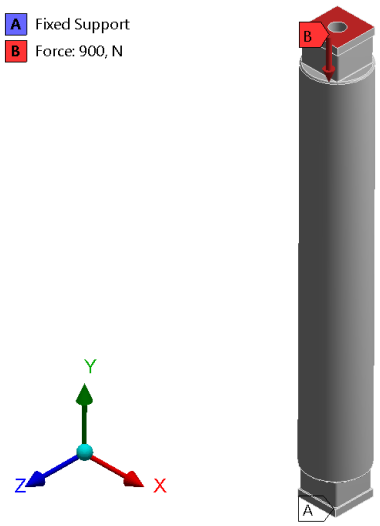

Fig. 13.- Load scenario and boundary conditions of the numerical simulations.

In order to discretize the geometry of the mechanical element under study solid structural tetrahedral elements of the type SOLID 92 were used. These elements have a quadratic displacement behavior, they are composed of 10 nodes (4 nodes in the vertices of the tetrahedron and 6 nodes in the midpoints of the same) and have three degrees of freedom in each node: translation in the Nodal X, Y and Z directions. To define the mesh a sizing operation is used that determines the approximate size of each element of the mesh, the section size being 2 mm. Fig. 14 shows the mesh used in the numerical simulations and Table 8 the statistics of the same. Finally it should be noted that, given the modeling of the PLA plastic material used for the numerical simulations carried out the option of Large displacement in the Solver definition has been activated to ensure that the final solution of the numerical model converges.

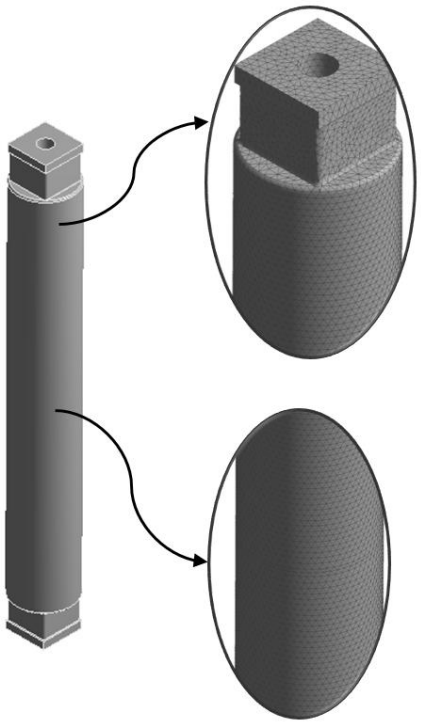

Fig. 14.- Mesh generated for mechanical simulation.

Nunmber of elements	251.298
Number of nodes	159.494
Element quality (Average)	0,850

Table 8.-Statistics of the mesh generated for thermal modeling.

5. Results and discussion

The data of uniaxial compression force and nominal displacements (see Fig.11) for the experimental test of the mechanical element under study show that the structural behavior is not compromised for the load scenario and boundary conditions to which it is subjected. According to the agricultural application of the mechanical assembly in which the mechanical element under study is included, the element is subjected to a uniaxial compression force of 900 N applied at one end of its geometry, and supported by a fixed articulation to the mechanical assembly at the opposite end to the load application (see Fig.3). As shown in Fig.11 and Fig.12, for a uniaxial compression force of 900 N the mechanical element under study has a nominal displacement of 0,3288 mm, a nominal deformation of 0,0011 mm/mm and a stress state of 2,598 MPa. As can be seen, the structural behavior for the mechanical stress to which the mechanical element is subjected is far from its state of collapse or breakage. The state of collapse or rupture of the mechanical element is reached for a uniaxial compression force of 16091.0 N (see Table 7), a value much higher than the load scenario to which the mechanical element is subjected during its nominal operating. In this way, the use of PLA plastic material is validated as well as the manufacturing process by means of additive manufacturing techniques of the FDM type for the mechanical element under study, according to its nominal operating presented in this article.

In accordance with the ISO-604 standard, used for characterizing the compressive elastic properties of PLA plastic material, the maximum nominal deformation used to determine the elastic properties of the material must accomplish the inequality presented in Eq.7

$$\varepsilon_c^* \leq 0{,}4 \cdot \frac{T_s^2}{L_s^2} \rightarrow 0{,}0025 \leq 0{,}4 \cdot \frac{4^2}{50^2} = 0{,}0026 \tag{7}$$

Eq.7 is defined by the geometrical characteristics of the specimens used for the material characterization. Where ε^*_c represents the nominal maximum deformation used for determining the elastic properties of the material, L_s [mm] represents the length of the specimens and T_s [mm] represents the thickness of the specimens. As can be seen (see Eq.7) the restriction imposed by the ISO-604 standard is fulfilled since the maximum nominal deformation used for the characterization of the compression Young modulus is 0,0025 (less than 0,0026, the deformation obtained in the second member of the inequality Eq.7)

The domain of the polynomial function (and therefore of the elastic region of the curve imported into the numerical simulation software) in the numerical simulation is limited by a range of nominal deformations between 0 and 0,0026 mm (as determined by standard ISO-604). It should be mentioned that the numerical simulation has been carried out from the polynomial function that interpolates the uniaxial compression stress curve against the nominal deformations.

Fig.15 shows the displacement field for the mechanical stress analyzed in this paper (see Fig.3 and Fig.13), obtained by means of two types of numerical simulations performed on the mechanical element under study. In the first type of numerical simulation the maximum displacement at the end point where the uniaxial compression load is applied has a value of 0,31475 mm. This maximum displacement occurs in the area where the plastic material PLA is characterized as isotropic from its elastic properties. In this area the Young modulus compression equals 2528.5 MPa. In the second type of numerical simulation PLA plastic material is characterized by importing the points of the polynomial function. The results of the second simulation point to the maximum displacement value (in the direction where the load is applied) obtained at the end where the uniaxial compression load of value 0,32761 mm is applied. In the second simulation the polynomial function interpolates the elastic regime of the uniaxial compression stress curve versus nominal strain (see Fig.8) obtained in the experimental tests of the specimens. Comparing these numerical results with the experimental result, it is verified that the numerical model that uses the polynomial function that interpolates the uniaxial compression stress curve versus nominal strain (Case B, see Fig.15) is closer to the experimental solution with an error of 0,36%. For the numerical model where the material is defined as isotropic with compression Young modulus constant (Case A, see Fig.15), the error in the numerical solution is 4.27% with respect to the experimental solution.

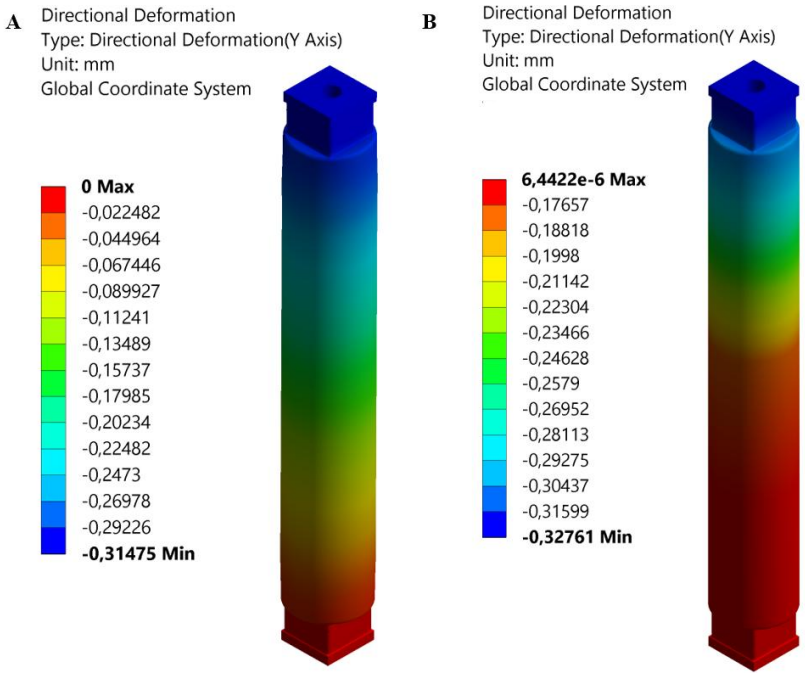

Fig. 15.- Field of displacements obtained in the mechanical simulations. a) Compression Young modulus Ec = 2528.5 MPa. b) Importation of the polynomial function that interpolates the elastic region of the uniaxial curve compression stress vs. nominal strain curve.

In this way, it is verified that in order to numerically analyze the structural behavior of a mechanical element subjected to a tensional state of uniaxial compression the plastic material PLA for 3D printing by means of FDM techniques can be modeled numerically as an isotropic material. This is possible from the importation to the numerical calculation software of the polynomial function that interpolates the elastic regime of the uniaxial compression stress curve versus nominal strain for that material. That is, based on a structural analysis in the elastic region of the plastic material it can be considered and modeled numerically as an isotropic material and the elastic properties can be defined from the experimental results of the specimens tested according to ISO standard-604. In addition, this type of numerical modeling of the material is easier to define in the numerical simulation software, since it does not require the modification of the constitutive equations in the material database and choosing the right material orientation in the numerical model. However, outside the elastic regime anisotropic material properties should be considered for the numerical model of the material.

Finally, it should be noted that the magnitude of the compression yield stress parameter obtained in the experimental tests both for the specimens (see Table 6) and for the mechanical element under study (see Table 7) are analogous. The compression yield stress obtained for the tested specimens is equal to 44.2 MPa (see Fig.8), while the compression yield stress for the mechanical element under study is 48.78 MPa (see Fig.12). However, the fracture process of PLA plastic material is different for the geometry of the specimens and for the geometry of the mechanical element under study. That is, the magnitude of the compression fracture stress parameter differs since in the experimental tests of the specimens the value is 28.3 MPa while in the mechanical element under study the value is 48.47 MPa. As shown in Fig. 12, the compression fracture stress is close to the compression yield stress, which means that the geometry and circular ring-shaped section of the mechanical element under study has a brittle fracture of the PLA plastic material. That is, the plastic deformation after reaching the compression yield stress until the compression fracture stress is very small or even negligible. On the other hand, Fig.8 shows that the compression yield stress of the PLA material for the geometry of the specimens tested is far from the compression fracture stress. This implies that for the prismatic geometry of the specimens there is a more noticeable plastic deformation despite having a completely brittle breakage caused by the rupture and separation between the different layers of the printed plastic material (see Fig.9). This may be due to the fact that the specimens tested and the mechanical element under study have different geometry and cross section (despite sharing the same parameters in manufacturing using FDM additive techniques). Therefore, as in the present work, both tests can be compared only for the elastic region of the plastic material for 3D printing PLA.

6. Conclusions

The work presented in this paper shows the mechanical properties of FDM structures manufactured with PLA that are subject to stress fields of uniaxial compression. The results have been validated through experimental tests and numerical simulations using test specimens and FDM end-parts. The results show good accuracy between the virtual and physical models. A first experimental test according to the conditions and requirements established in the ISO-604 standard allows us to characterize the mechanical and elastic properties of PLA material manufactured with FDM technology when it is in a uniaxial compression stress state. A second experimental test has analyzed the structural behavior of the object of study consisting of a hollow bar for agricultural machinery applications, evaluating the compression stiffness of the mechanical element, the compression yield stress, the field of displacements and stresses along its elastic behavior until reaching the compression yield stress and the ultimate yield stress. The information of the experimental model has been used for the realization of a set of numerical simulations with different elastic models for the mechanical element object of study, validating the physical model. The characterization of the elastic zone for the PLA material manufactured with FDM has been used to simulate numerically the study case by means of two empirical models. The first of the models uses the interpolation of experimental data to obtain the polynomial function of the uniaxial stress-compression curve versus nominal deformations while the second model uses the Young's modulus to compression according to the guidelines established in ISO standard 604. The fracture produced in the test specimens is of a brittle type since it is not produced by collapse of the plastic material but by separation between the central layers of the plastic filament.

The analysis of the results obtained indicates that the structural study of the elastic region of the plastic material PLA manufactured with FDM can be modeled numerically as an isotropic material, defining the elastic properties of the same from the experimental results of the specimens tested according to ISO standard 604. This type of numerical modeling of the material is easy to define in the numerical calculation software, since it does not require modification of the constitutive equations in the material database as well as the selection of the right material orientation. The data of uniaxial compression force as well as the nominal displacements for the experimental test and the numerical simulations of the object of study, show that its structural behavior is not compromised for the load scenario and boundary conditions to which it is subjected. In this way, the use of PLA plastic material and the FDM manufacturing

process for the mechanical element under study according to the nominal operation presented in the article is validated. The element designed is biodegradable and can be manufactured by the farmer himself who can repair it autonomously when needed without depending on the deadlines given by the supplier. Additionally, its advantage is its sustainability and respect for the environment in its life cycle, complying with the circular economy concept in the field of sustainable manufacturing

7. Acknowledgments

This work has been supported by the University of Jaen through the project titled " Design of a mechanical plastic device for the displacement of collection sheets for olive harvesting" Project Code (AC20/2016-10) and (ID228-R2 A8 2018).

8. References

[1] Primo, T., Calabrese, M., Del Prete, A., & Anglani, A. (2017). Additive manufacturing integration with topology optimization methodology for innovative product design. *The International Journal of Advanced Manufacturing Technology*, *93*(1-4), 467-479.

[2] Leary, M., Merli, L., Torti, F., Mazur, M., & Brandt, M. (2014). Optimal topology for additive manufacture: a method for enabling additive manufacture of support-free optimal structures. *Materials & Design*, *63*, 678-690.

[3] Mercado-Colmenero, J. M., Paramio, M. R., Perez-Garcia, J. M., & Martin-Doñate, C. (2016). A new hybrid method for demoldability analysis of discrete geometries. *Computer-Aided Design*, *80*, 43-60.

[4] Mercado-Colmenero, J. M., Muriana, J. A. M., Rubio-Paramio, M. A., & Martín-Doñate, C. (2017). An automated manufacturing analysis of plastic parts using faceted surfaces. In *Advances on Mechanics, Design Engineering and Manufacturing* (pp. 119-128). Springer, Cham.

[5] Doñate, C. M., & Paramio, M. R. (2013). New methodology for demoldability analysis based on volume discretization algorithms. *Computer-Aided Design*, *45*(2), 229-240

[6] Thompson, M. K., Moroni, G., Vaneker, T., Fadel, G., Campbell, R. I., Gibson, I. & Martina, F. (2016). Design for Additive Manufacturing: Trends, opportunities, considerations, and constraints. CIRP annals, 65(2), 737-760.

[7] Mercado-Colmenero, J. M., Rubio-Paramio, M. A., Guerrero-Villar, F., & Martin-Doñate, C. (2018). A numerical and experimental study of a new Savonius wind rotor adaptation based on product design requirements. *Energy Conversion and Management*, *158*, 210-234.

[8] Zhai, Y., Lados, D. A., & LaGoy, J. L. (2014). Additive manufacturing: making imagination the major limitation. Jom, 66(5), 808-816.

[9] Wohlers, T. (2012). *Wohlers report 2012*. Wohlers Associates, Inc.

[10] Puigoriol-Forcada, J. M., Alsina, A., Salazar-Martín, A. G., Gomez-Gras, G., & Pérez, M. A. (2018). Flexural Fatigue Properties of Polycarbonate Fused-deposition Modelling Specimens. *Materials & Design*.

[11] Stephens, B., Azimi, P., El Orch, Z., & Ramos, T. (2013). Ultrafine particle emissions from desktop 3D printers. *Atmospheric Environment*, *79*, 334-339.

[12] Pearce, J. M. (2015). Applications of open source 3-D printing on small farms. *Organic Farming*

[13] Kaltoft, P. (1999). Values about nature in organic farming practice and knowledge. *Sociologia ruralis*, *39*(1), 39-53.

[14] Watson, C. A., Atkinson, D., Gosling, P., Jackson, L. R., & Rayns, F. W. (2002). Managing soil fertility in organic farming systems. *Soil use and management*, *18*, 239-247.

[15] Stockdale, E. A., Shepherd, M. A., Fortune, S., & Cuttle, S. P. (2002). Soil fertility in organic farming systems–fundamentally different?. *Soil use and management*, *18*, 301-308.

[16] Levanon, D., & Pluda, D. (2002). Chemical, physical and biological criteria for maturity in composts for organic farming. Compost Science & Utilization, 10(4), 339-346.

[17] Caulfield, B., McHugh, P. E., & Lohfeld, S. (2007). Dependence of mechanical properties of polyamide components on build parameters in the SLS process. *Journal of Materials Processing Technology*, *182*(1-3), 477-488.

[18] Tymrak, B. M., Kreiger, M., & Pearce, J. M. (2014). Mechanical properties of components fabricated with open-source 3-D printers under realistic environmental conditions. *Materials & Design*, *58*, 242-246.

[19] Baumers, M., Duflou, J. R., Flanagan, W., Gutowski, T. G., Kellens, K., & Lifset, R. (2017). Charting the environmental dimensions of additive manufacturing and 3D Printing. *Journal of Industrial Ecology*, *21*(S1), S9-S14.

[20] Casavola, C., Cazzato, A., Moramarco, V., & Pappalettere, C. (2016). Orthotropic mechanical properties of fused deposition modelling parts described by classical laminate theory. *Materials & design*, *90*, 453-458.

[21] Mohamed, O. A., Masood, S. H., & Bhowmik, J. L. (2015). Optimization of fused deposition modeling process parameters: a review of current research and future prospects. *Advances in Manufacturing*, *3*(1), 42-53.

[22] Domingo-Espin, M., Puigoriol-Forcada, J. M., Garcia-Granada, A. A., Lluma, J., Borros, S., & Reyes, G. (2015). Mechanical property characterization and simulation of fused deposition modeling Polycarbonate parts. *Materials & Design*, *83*, 670-677

[23] Wu, W., Geng, P., Li, G., Zhao, D., Zhang, H., & Zhao, J. (2015). Influence of layer thickness and raster angle on the mechanical properties of 3D-printed PEEK and a comparative mechanical study between PEEK and ABS. *Materials*, *8*(9), 5834-5846

[24] Ulu, E., Korkmaz, E., Yay, K., Ozdoganlar, O. B., & Kara, L. B. (2015). Enhancing the structural performance of additively manufactured objects through build orientation optimization. *Journal of Mechanical Design*, *137*(11), 111410.

[25] Vaezi, M., & Chua, C. K. (2011). Effects of layer thickness and binder saturation level parameters on 3D printing process. *The International Journal of Advanced Manufacturing Technology*, *53*(1-4), 275-284.

[26] Anitha, R., Arunachalam, S., & Radhakrishnan, P. (2001). Critical parameters influencing the quality of prototypes in fused deposition modelling. *Journal of Materials Processing Technology*, *118*(1-3), 385-388.

[27] Rodríguez, J. F., Thomas, J. P., & Renaud, J. E. (2001). Mechanical behavior of acrylonitrile butadiene styrene (ABS) fused deposition materials. Experimental investigation. *Rapid Prototyping Journal*, *7*(3), 148-158

[28] Matsuzaki, R., Ueda, M., Namiki, M., Jeong, T. K., Asahara, H., Horiguchi, K., ... & Hirano, Y. (2016). Three-dimensional printing of continuous-fiber composites by in-nozzle impregnation. *Scientific reports*, *6*, 23058.

[29] Sood, A. K., Ohdar, R. K., & Mahapatra, S. S. (2010). Parametric appraisal of mechanical property of fused deposition modelling processed parts. *Materials & Design*, *31*(1), 287-295.

[30] Lanzotti, A., Grasso, M., Staiano, G., & Martorelli, M. (2015). The impact of process parameters on mechanical properties of parts fabricated in PLA with an open-source 3-D printer. *Rapid Prototyping Journal*, *21*(5), 604-617.

[31] Rodríguez, J. F., Thomas, J. P., & Renaud, J. E. (2003). Design of fused-deposition ABS components for stiffness and strength. *Journal of Mechanical Design*, *125*(3), 545-551.

[32] Ahn, S. H., Montero, M., Odell, D., Roundy, S., & Wright, P. K. (2002). Anisotropic material properties of fused deposition modeling ABS. *Rapid prototyping journal*, *8*(4), 248-257.

[33] Lee, B. H., Abdullah, J., & Khan, Z. A. (2005). Optimization of rapid prototyping parameters for production of flexible ABS object. *Journal of materials processing technology*, *169*(1), 54-61.

[34] Croccolo, D., De Agostinis, M., & Olmi, G. (2013). Experimental characterization and analytical modelling of the mechanical behaviour of fused deposition processed parts made of ABS-M30. *Computational Materials Science*, *79*, 506-518.

[35] Casavola, C., Cazzato, A., Moramarco, V., & Pappalettera, G. (2017). Residual stress measurement in fused deposition modelling parts. *Polymer Testing*, *58*, 249-255.

[36] Tanikella, N. G., Wittbrodt, B., & Pearce, J. M. (2017). Tensile strength of commercial polymer materials for fused filament fabrication 3D printing. *Additive Manufacturing*, *15*, 40-47.

[37] Kuznetsov, V. E., Solonin, A. N., Urzhumtsev, O. D., Schilling, R., & Tavitov, A. G. (2018). Strength of PLA Components Fabricated with Fused Deposition Technology Using a Desktop 3D Printer as a Function of Geometrical Parameters of the Process. Polymers, 10(3), 313.

[38] Wittbrodt, B., & Pearce, J. M. (2015). The effects of PLA color on material properties of 3-D printed components. *Additive Manufacturing*, *8*, 110-116

[39] Chacón, J. M., Caminero, M. A., García-Plaza, E., & Núñez, P. J. (2017). Additive manufacturing of PLA structures using fused deposition modelling: Effect of process parameters on mechanical properties and their optimal selection. *Materials & Design*, *124*, 143-157.

[40] Torres, J., Cotelo, J., Karl, J., & Gordon, A. P. (2015). Mechanical property optimization of FDM PLA in shear with multiple objectives. *Jom*, *67*(5), 1183-1193.

[41] Uddin, M. S., Sidek, M. F. R., Faizal, M. A., Ghomashchi, R., & Pramanik, A. (2017). Evaluating mechanical properties and failure mechanisms of fused deposition modeling acrylonitrile butadiene styrene parts. *Journal of Manufacturing Science and Engineering*, *139*(8), 081018.

[42] Upadhyay, K., Dwivedi, R., & Singh, A. K. (2017). Determination and comparison of the anisotropic strengths of fused deposition modeling P400 ABS. In Advances in 3D Printing & Additive Manufacturing Technologies (pp. 9-28). Springer, Singapore.

[43] Sood, A. K., Ohdar, R. K., & Mahapatra, S. S. (2012). Experimental investigation and empirical modelling of FDM process for compressive strength improvement. *Journal of Advanced Research*, *3*(1), 81-90.

[44] Lee, C. S., Kim, S. G., Kim, H. J., & Ahn, S. H. (2007). Measurement of anisotropic compressive strength of rapid prototyping parts. *Journal of materials processing technology*, *187*, 627-630.

[45] Popescu, D., Zapciu, A., Amza, C., Baciu, F., & Marinescu, R. (2018). FDM process parameters influence over the mechanical properties of polymer specimens: A review. *Polymer Testing*, *69*, 157-166.

[46] https://www.progressiveforage.com/forage-production/equipment/3-d-printing-in-agriculture

[47]https://www.aitiip.com/noticias/como-una-impresora-3d-ayudo-a-un-agricultor-a-no-perder-su-cosecha-de-trigo.html

[48] https://www.mmtimes.com/business/technology/24364-farmers-reap-rewards-from-3d-printing.html

[49]. Martín-Doñate, C; Rubio-Paramio M.A ; Gómez-García J. J., García Tamargo J. González Lozano I. Toledano Rama I. .Mechanical device for the displacement of collection sheets for olive harvesting Patent Request Number P201830843. 2018

[50] https://smartmaterials3d.com/es/

[51] https://ultimaker.com/en/products/ultimaker-2-plus

[52] https://www.iso.org/standard/31261.html

[53] https://www.ansys.com/products/structures

Vitae

Jorge Manuel Mercado Colmenero received his B.Eng and M.Eng. in Mechanical Engineering in 2012 and 2014 respectively from the University of Jaén in Spain. In 2014 he joined the Design, Engineering Graphics and Project department at Jaen university as a PhD student. He is currently developing his thesis on automatic analyses and design of injection plastic molds, including demoldability, ejection systems, cooling system design and CAD-CAE design and manufacturing. He carried out research at the Politecnico di Bari in Italy in the field of injection molding and industrial design.

Prof. Dr. Miguel Angel Rubio Paramio received his M.Eng. and Ph.D in Mechanical Engineering in 1992 and 2000 respectively from the Polytechnic University of Madrid in Spain. In 1994 he joined the University of Jaen and he holds the position of head of the department of Engineering Graphics, Design and Proyects since 2014. He currently teaches courses on Computer-aided Design, Manufacturing and Engineering in the Engineering Graphics, Design and Projects Department. His thesis was focused on the automatic analysis of plastic parts injection. His research interests include CAD– CAM–CAE, Design for Manufacturing, computational geometry, constraint-based parametric modeling, and their applications in plastic injection mold design and manufacturing.

Prof. Dr. Mª Dolores La Rubia García received her Degree in Chemical Sciences from the University of Jaén-Spain , Master in Science and Technology of Polymers from the UNED-Spain and PhD in Chemical Sciences (University of Jaén - Spain). She is currently Professor at the University of Jaen where she develops research on Advanced Materials and Bioprocesses.

David Lozano Arjona received his B.Eng in Mechanical Engineering from the University of Jaen in Spain and M. Eng in Automotive Engineering from the TU in Aachen in Germany. In 2017 he joined the Design, Engineering Graphics and Project Department at Jaen University as a PhD student. He is currently involved with several projects related Automotive Engineering.

Prof. Dr. Cristina Martín Doñate received her B.Eng. and M.Eng. in Electrical - Electronics Engineering and Industrial Engineering (Polytechnic University of Valencia - Spain) and Ph.D in Industrial Engineering (University of Jaen - Spain). She carried out research at the Technical University of Graz in Austria, at the University of Applied sciences of Rosenheim in Germany and at the Politecnico di Bari in Italy in the field of manufacturing systems, injection molding and industrial design. She worked for several years as a project manager developing new products in the automotive manufacturing industries. She is currently Professor at the University of Jaen where she develops research and conducts research projects into manufacturing systems, plastic injection mold design and technology, additive manufacturing, CAD systems and new products development.

Table1

PLA Properties	Value	Units
Density	1,24	g/cm^3
Tensile strength MD	110	MPa
Tensile strength TD	114	MPa
Tensile modulus MD	3309	MPa
Tensile modulus TD	3861	MPa
Elongation at break MD	160	%
Elongation at break TD	100	%
Heat deflection temperature	65	ºC
Vicat softering temperature	85	ºC
Print temperature	220±10	ºC
Hot pad	0-60ºC	ºC

Table 1.- Physical, mechanical and printing properties for PLA material manufactured with FDM technology.

Table2

Variable	Description	Units	Value
$Ø_e$	Outer diameter of the mechanical element	mm	40
$Ø_i$	Inner diameter of the mechanical element	mm	34
L	Length of the mechanical element	mm	300

Table 2.- Geometrical variables that define the mechanical element under study.

Table3

Manufacturing parameters	Value	Units
Layer height	0,2	mm
Nozzle size	0,4	mm
Infill density	100	%
Print speed	50	mm/s
Travel speed	120	mm/s

Table 3.- Parameters of manufacture used for the manufacture of the elements of the present study.

Table4

Measurement parameter	Length, L_s	Weidth, W_s	Thickness, T_s	Unit
Compression Young modulus	50±2	10,0±0,2	4±0,2	Mm
Compression yield stress	50±2	10,0±0,2	4±0,2	Mm

Table 4.- Dimensions of the specimens used for the characterization of PLA compression material.

Table5

Interpolation parameters	Value
Coefficients (95% confidence bounds):	
P1	$-3{,}465 \cdot 10^{17}$
P2	$2{,}394 \cdot 10^{16}$
P3	$-6{,}613 \cdot 10^{14}$
P4	$9{,}253 \cdot 10^{12}$
P5	$-6{,}803 \cdot 10^{10}$
P6	$2{,}386 \cdot 10^{8}$
P7	$-2{,}266 \cdot 10^{5}$
P8	2131
P9	-0,004
Goodness of fit:	
SSE	113,1
R-Square	0,999
Adjusted R-Square	0,999
RMSE	0,2741

Table 5.- Results of the polynomial interpolation of the uniaxial curve compression stress against nominal deformations

Table6

Compression properties	Units	S1	S2	S3	S4	S5	S6	Arithmetic average	Typical deviation
Young modulus, E_c	MPa	2304,7	2363,3	2903,1	2319,0	2899,3	2381,3	2528,5	290,087
Yield stress, σ_y	MPa	44,09	40,59	46,08	42,99	46,72	44,77	44,2	2,223
Fracture stress, σ_f	MPa	40,76	20,94	31,58	28,05	25,54	22,73	28,3	7,196

Table 6.- Elastic and mechanical properties of PLA plastic material for each specimen.

Table8

Nunmber of elements	251.298
Number of nodes	159.494
Element quality (Average)	0,850

Table 8.-Statistics of the mesh generated for thermal modeling.

Figure1

Click here to download high resolution image

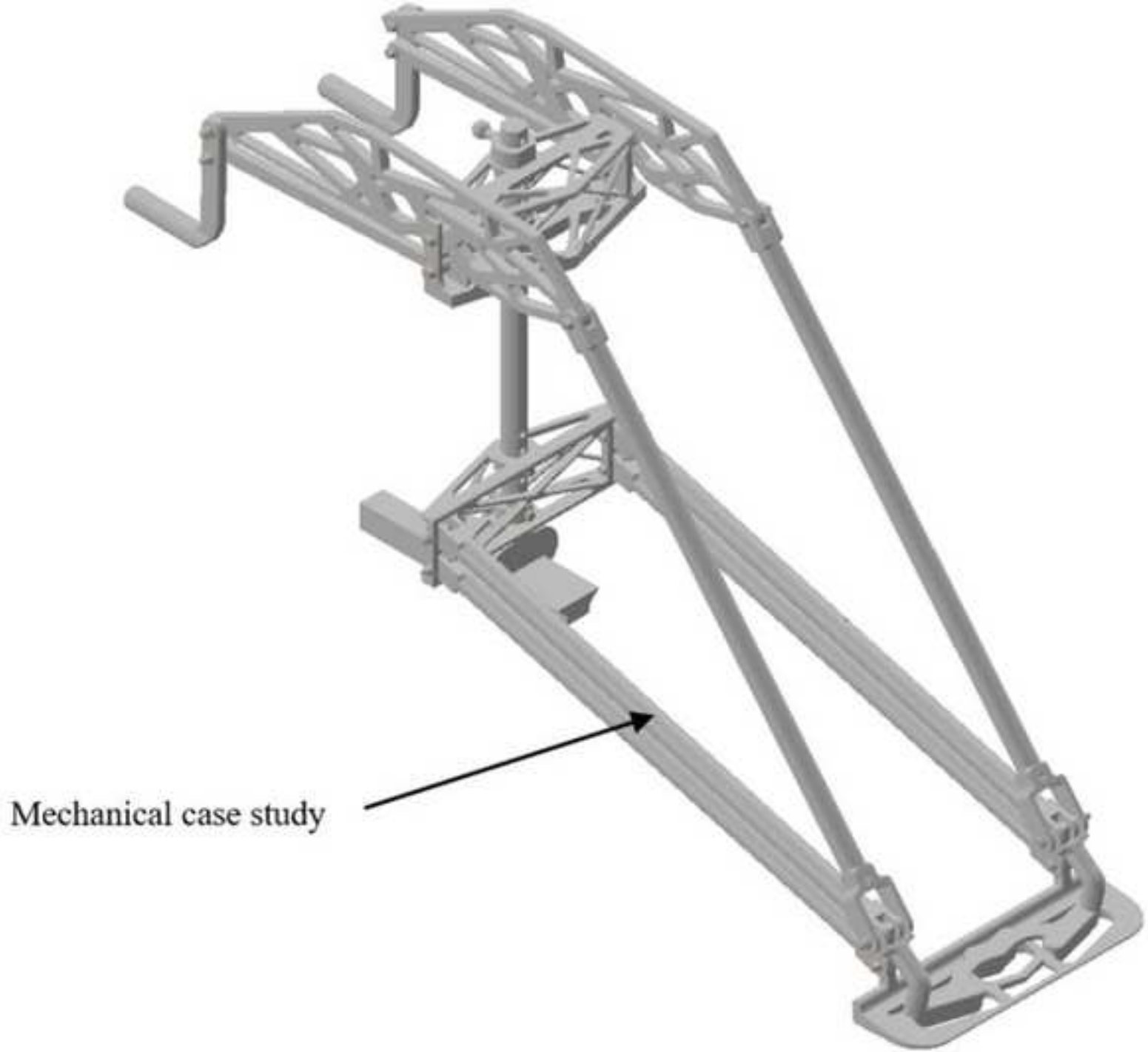

Figure2

Click here to download high resolution image

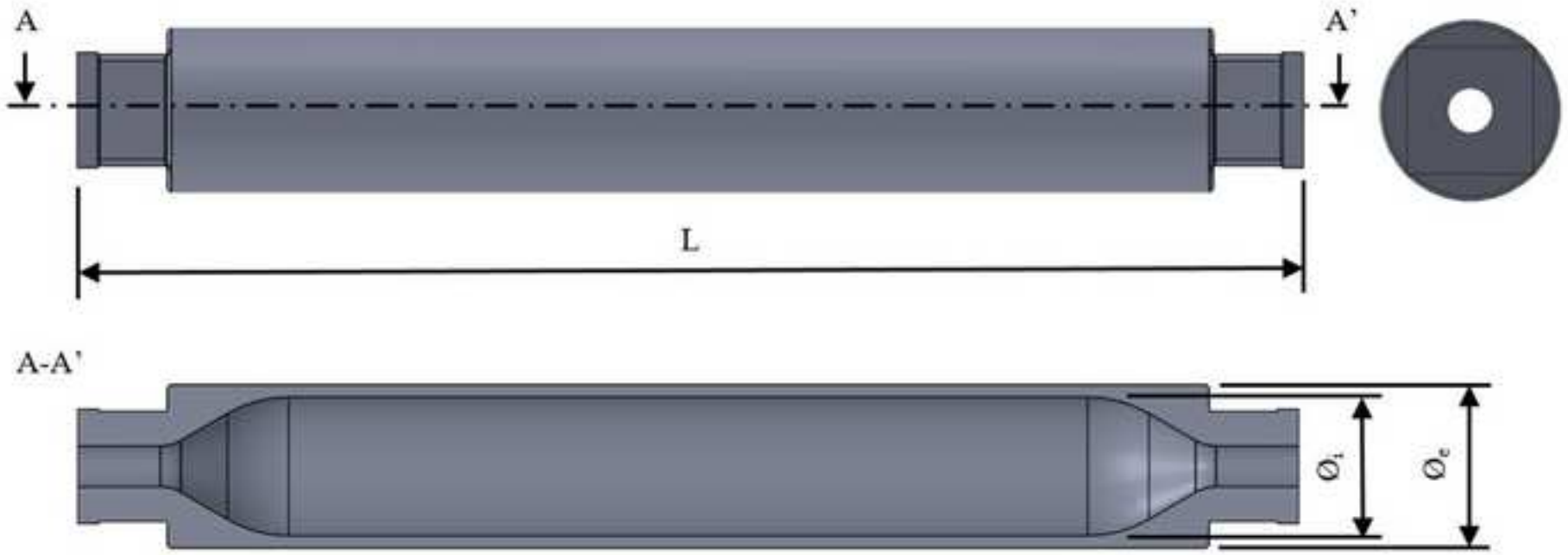

Figure3

Click here to download high resolution image

Figure4

Click here to download high resolution image

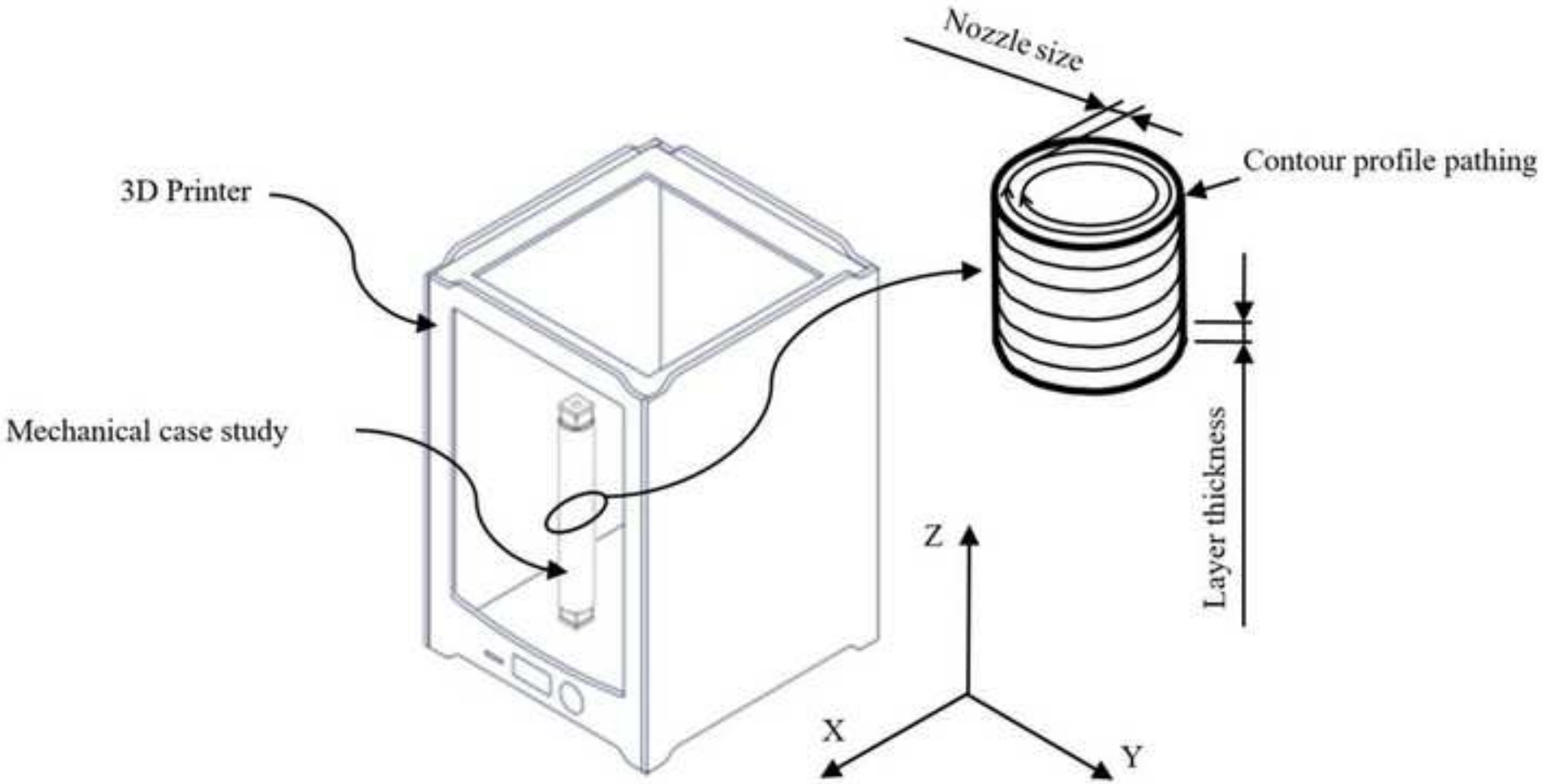

Figure5

Click here to download high resolution image

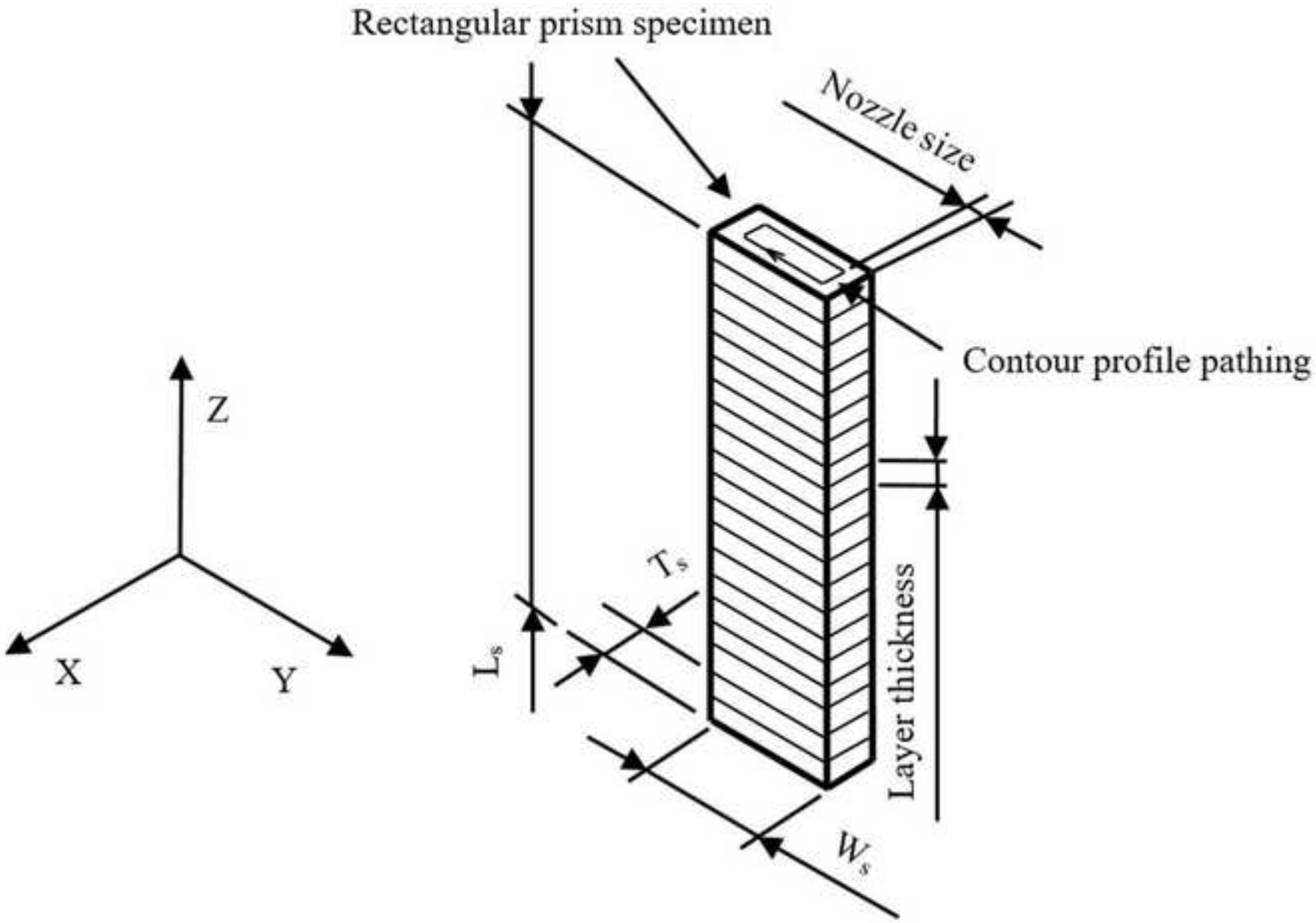

Figure6

Click here to download high resolution image

Figure7

Click here to download high resolution image

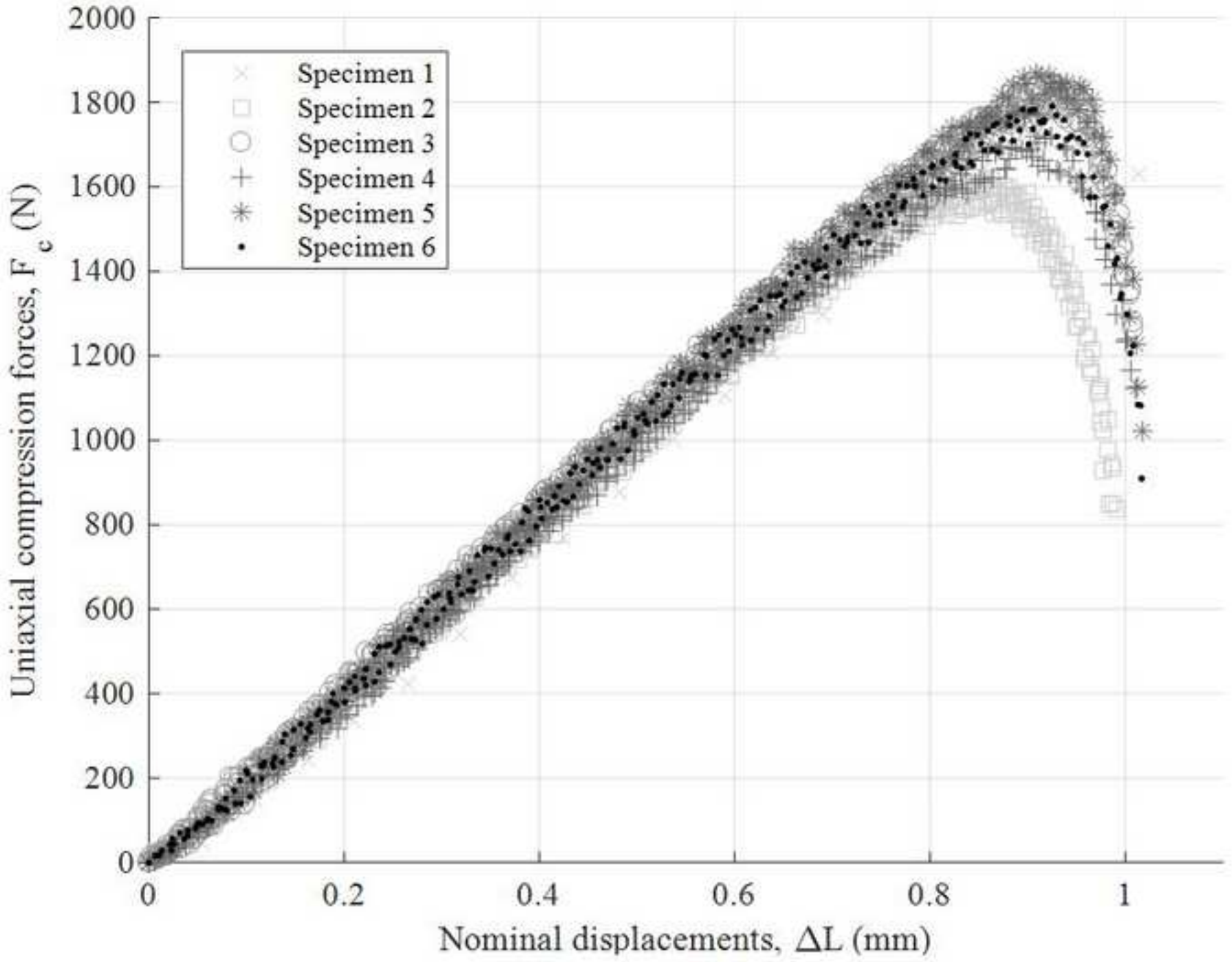

Figure8
Click here to download high resolution image

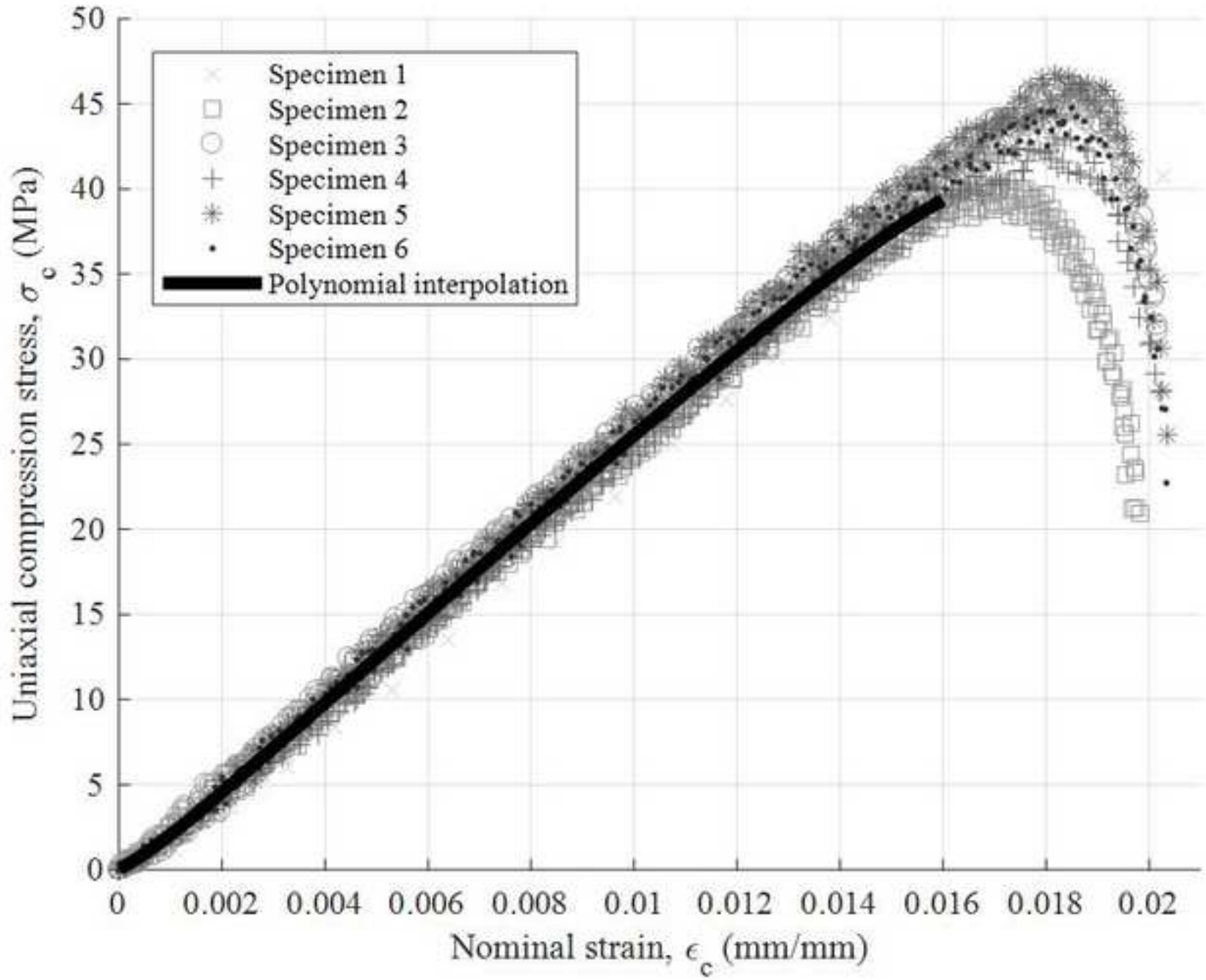

Figure9

Click here to download high resolution image

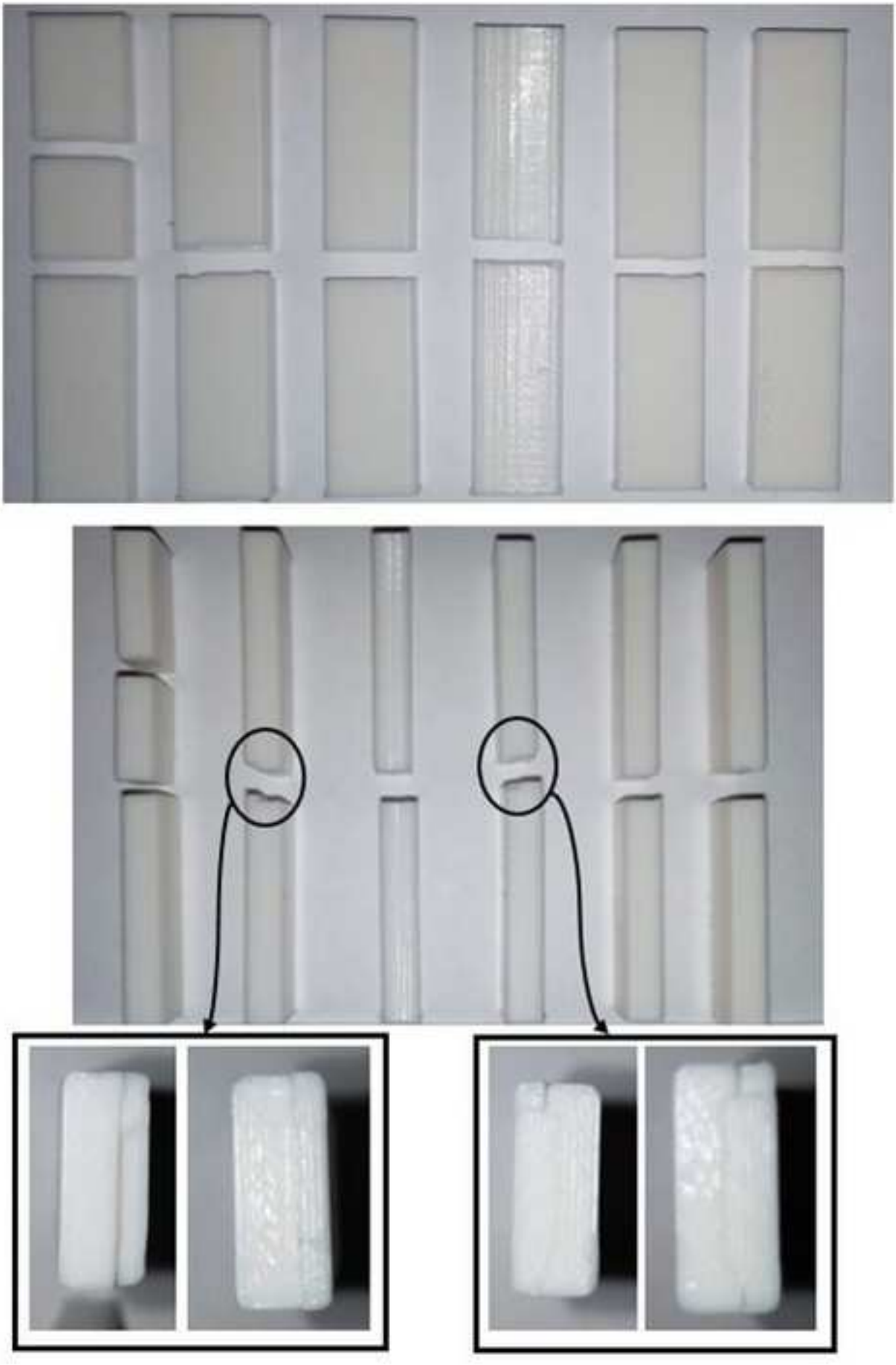

Figure11
Click here to download high resolution image

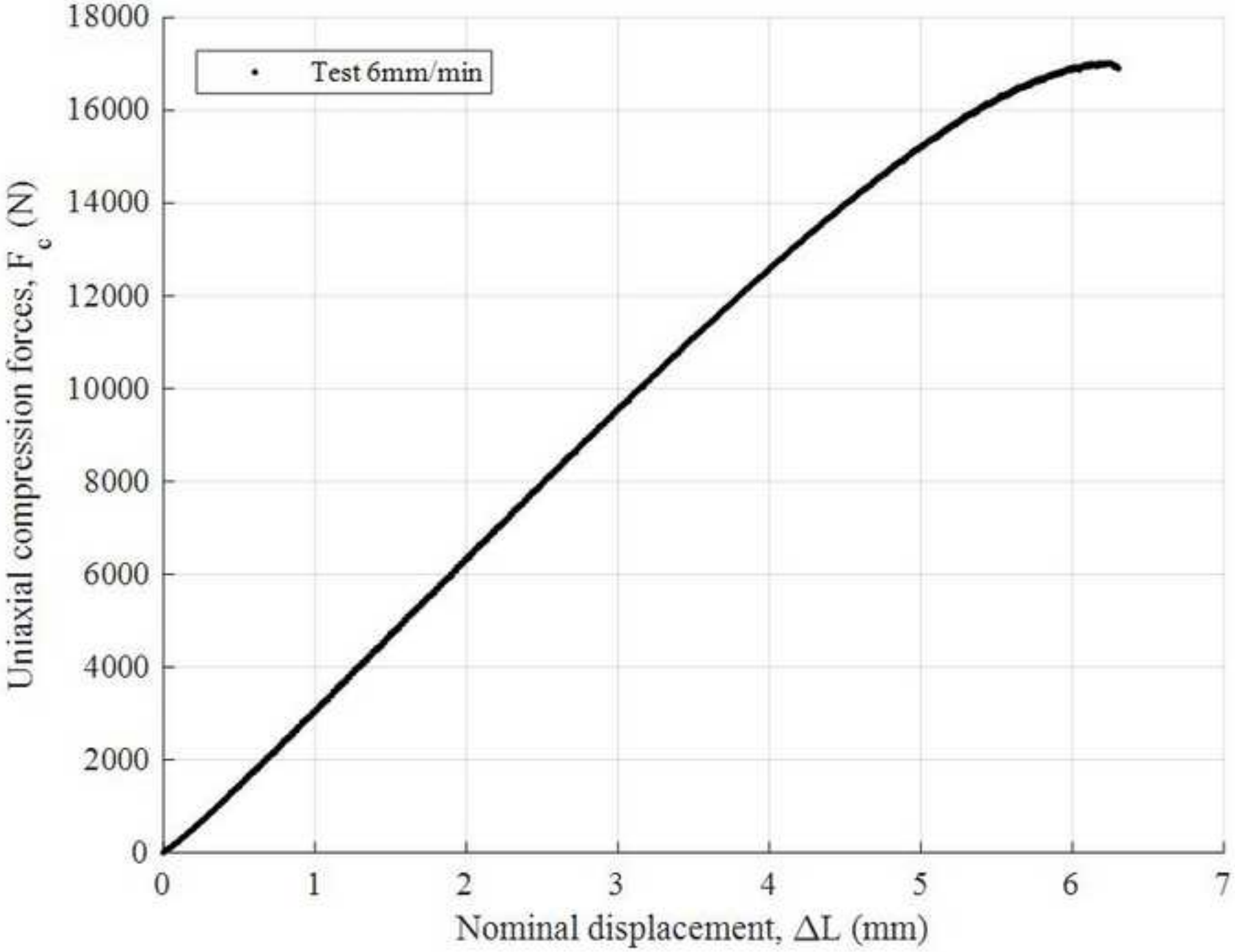

Figure12
Click here to download high resolution image

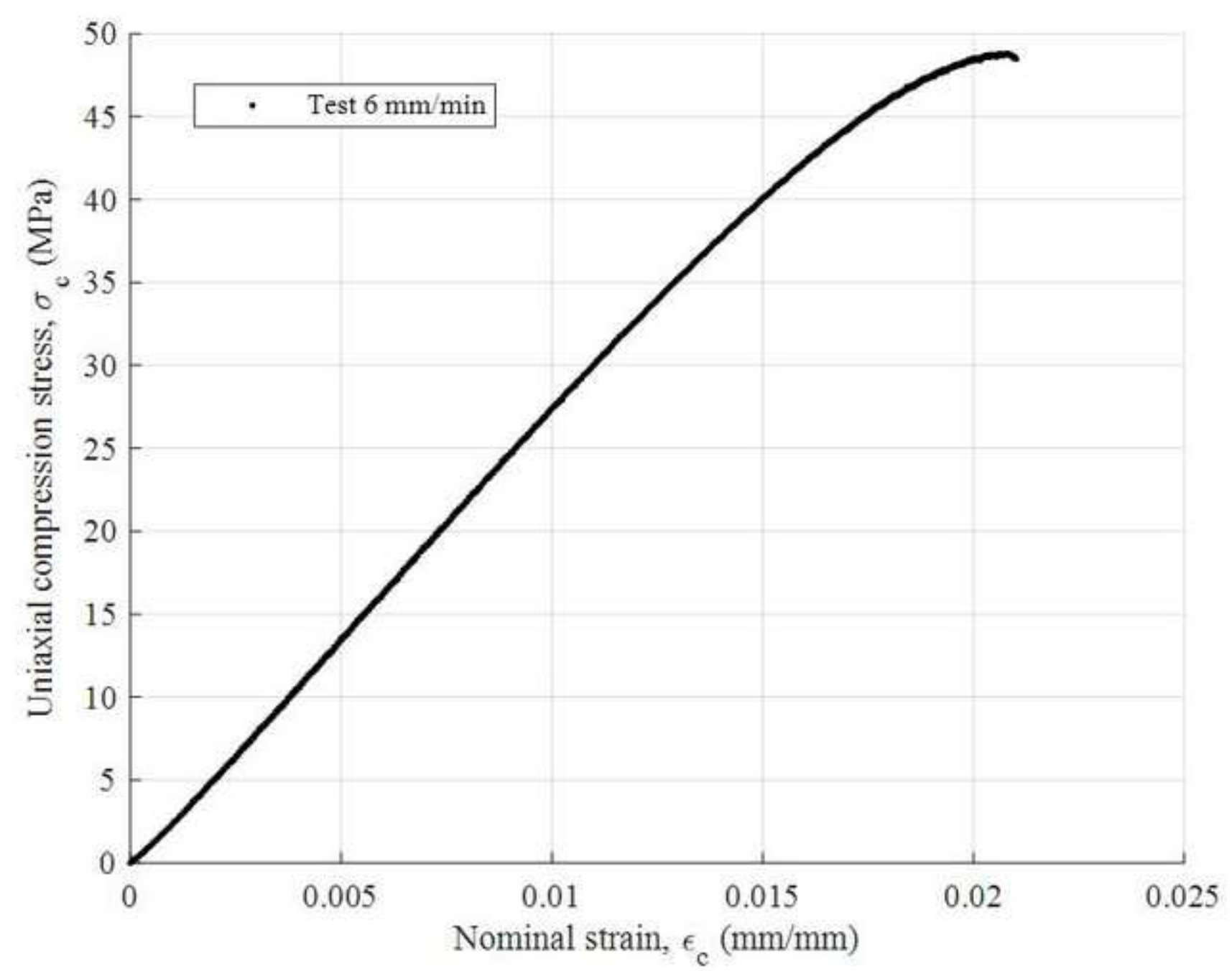

Figure13
Click here to download high resolution image

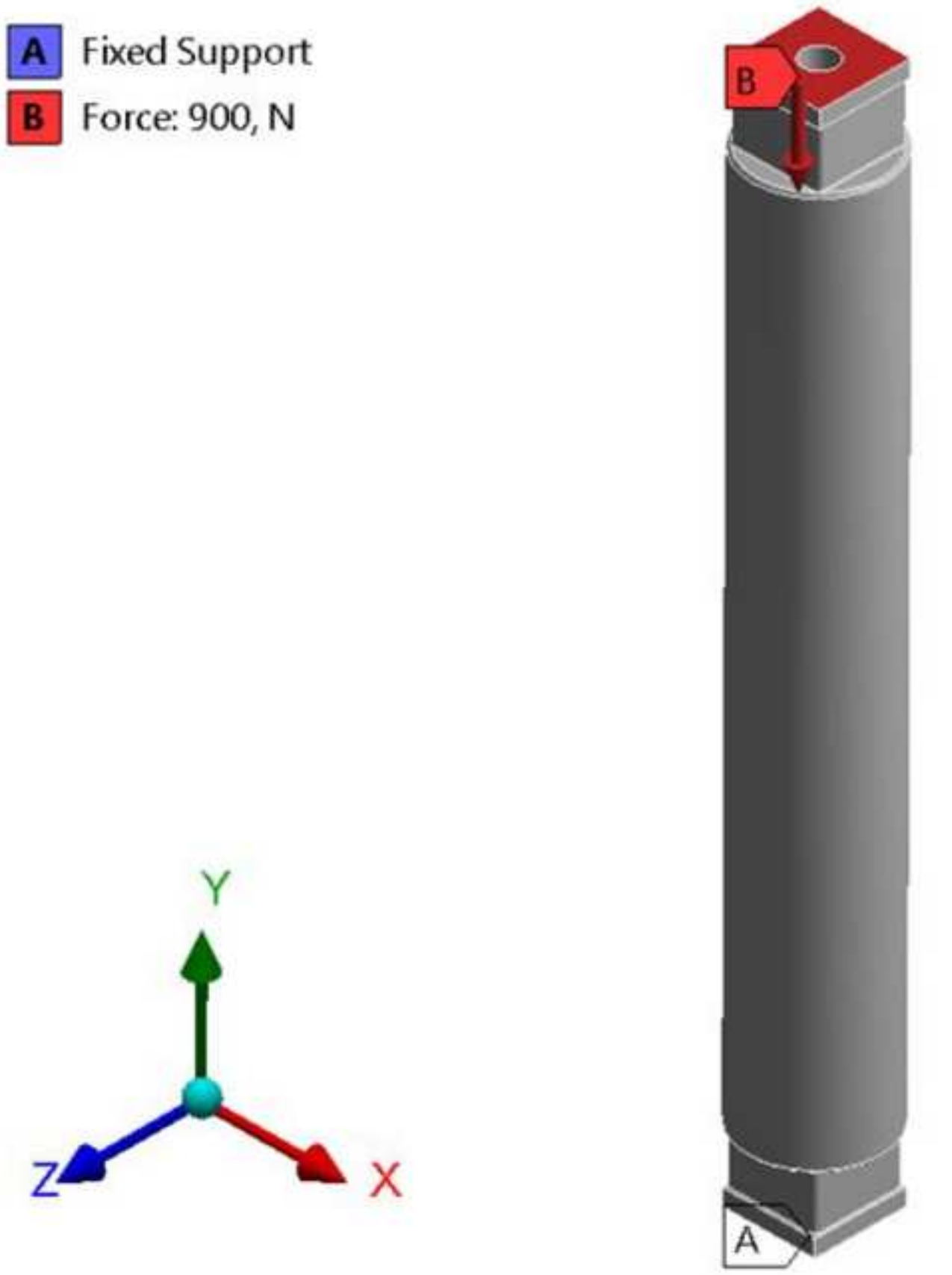

Figure14

Click here to download high resolution image

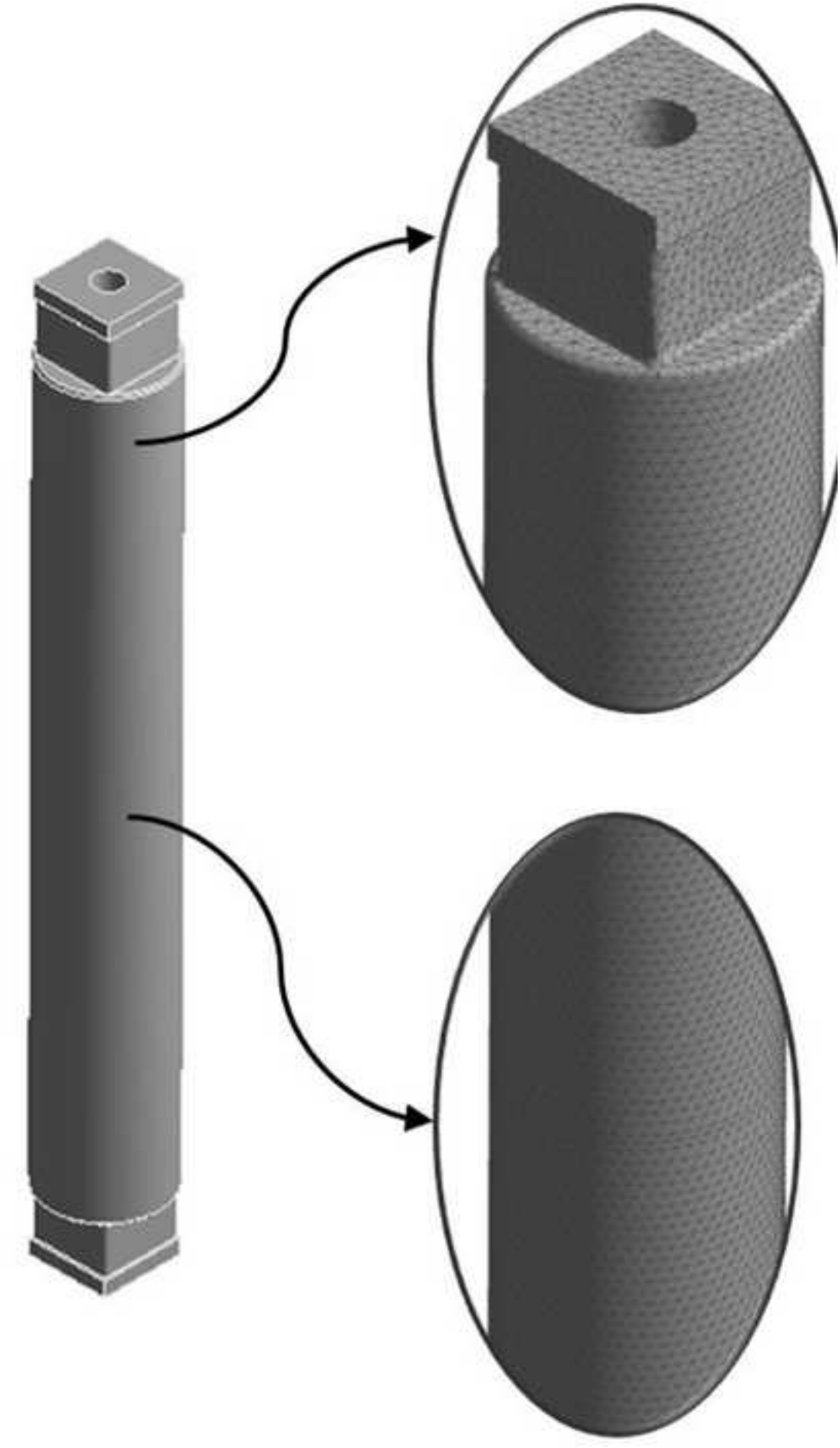

Figure15

Click here to download high resolution image